Vestiges of a fore-arc oceanic crust in the Western Mediterranean: Geochemical constraints from North-East Algeria

Laure Fernandez, Delphine Bosch, Olivier Bruguier, Dalila Hammor, Renaud Caby, Nicolas Arnaud, Patrick Monié, Nachida Abdallah, Patrick Verdoux, Aziouz Ouabadi, et al.

Research Article

Vestiges of a fore-arc oceanic crust in the Western Mediterranean: Geochemical constraints from North-East Algeria

Laure Fernandez [a], Delphine Bosch [a,*], Olivier Bruguier [a], Dalila Hammor [b], Renaud Caby [a], Nicolas Arnaud [a], Patrick Monié [a], Nachida Abdallah [c], Patrick Verdoux [d], Aziouz Ouabadi [c], Rabah Laouar [b,c]

[a] Géosciences Montpellier, Université de Montpellier, CNRS, Université des Antilles, Montpellier, France
[b] Laboratoire de Géologie, Université Badji-Mokhtar Annaba, BP12, 23000 Annaba, Algeria
[c] Laboratoire de Géodynamique, Géologie de l'Ingénieur et Planétologie, USTHB, BP32, Algiers, Algeria
[d] Laboratoire de Géochimie Isotopique environnementale, Université de Nîmes GIS, Nîmes, France

ARTICLE INFO

Article history:
Received 8 April 2020
Received in revised form 16 June 2020
Accepted 17 June 2020
Available online 24 June 2020

Keywords:
Western Mediterranean
Fore-arc
Alpine Tethys
Ligurian Ocean
Nd-Hf-Sr-Pb isotopes
Ar-Ar dating

ABSTRACT

The present day architecture of the Western Mediterranean mainly results from the interplay of different lithospheric plates and the Cenozoic consumption of various branches of the Alpine Tethys and Neo-Tethys Oceans. Identifying relics of these oceanic domains in the peri-Mediterranean belts enables pinpointing the earliest stages of this evolutionary framework. In NE Algeria, the Kef Lakhal Complex (Edough Massif) is composed of amphibolites and meta-gabbros metamorphosed under amphibolite facies conditions and thrust onto the northern African margin during earliest Miocene. Geochemical analyses reveal that amphibolites and metagabbros have major and trace element signatures characteristic of tholeiitic basalts and gabbros and display N-MORB ($La/Sm_N = 0.7–0.9$) to *E*-MORB ($La/Sm_N = 1.1–1.2$) affinities. Enrichments in U and alkalis (Cs, Rb) and high $^{87}Sr/^{86}Sr_i$ ratios on bulk rocks and minerals (up to 0.70856) are typical of seawater alteration and indicate that the Kef Lakhal Complex represents a piece of altered oceanic crust. Parental magmas were derived from a Depleted Mantle source (WR $\varepsilon Nd_i = 8.2–9.9$ and $\varepsilon Hf_i = 10.4–14.4$) that preserved some canonical MORB ratios ($Ti/Eu = 5700–7600$ and $Y/Ho = 27.4–29.0$), but which was contaminated by a component akin to recycled oceanic crust and associated sediments ($Ce/Pb = 10.5–22.2$; $^{206}Pb/^{204}Pb_i = 18.41–18.74$; $^{207}Pb/^{204}Pb_i = 15.49–15.59$; $^{208}Pb/^{204}Pb_i = 37.73–38.37$). The sedimentary component is consistent with a volcaniclastic origin and substantiates an intra-oceanic setting. The geochemical characteristics of the Kef Lakhal rocks are comparable to present day (Mariana, W Pacific Ocean) or fossil (Xigaze, SE Tibet) fore-arc oceanic crust. An overview of the Western Mediterranean geodynamic indicates that the most likely period for initiating formation of a fore-arc corresponds either to the Early/Late Cretaceous or to the Middle Eocene. $^{40}Ar/^{39}Ar$ dating on amphibole further indicate that after thrusting onto the African margin, the Kef Lakhal Complex cooled down to *c.*550 °C at 18.14 ± 0.27 Ma (2σ).

1. Introduction

Studies of mafic rocks preserved in the internal zones of orogenic belts are paramount for geodynamic reconstructions (e.g. Carminati et al., 2012) as they provide insights on the nature of the mantle sources from which they derive, on the mantle dynamics, as well as important constraints on their original geodynamical setting (e.g. McCulloch and Gamble, 1991). The Western Mediterranean represents a mosaic of continental and oceanic fragments arising from fragmentation of the Paleo-European margin (e.g. *AlKaPeCa* domain of Bouillin, 1986), tearing and eventually break-off of the Tethyan slab segments, along with the Cenozoic addition of new oceanic basins such as the Liguro-Provencal basin (LPB), the Algerian Basin or the Tyrrhenian Sea. In such a context, paleo-reconstructions rely on the resolution of key issues, such as the age of subduction, the beginning of slab retreat and associated processes, the possible formation of back-arc basins and the exhumation of HP/UHP rocks (e.g. Brun and Faccenna, 2008; Jolivet et al., 2013; van Hinsbergen et al., 2014). Study of mafic/ultramafic rocks preserved in the internal zones of the peri-Mediterranean belts can considerably help defining the processes and timing, hence limiting the variability of geodynamic models and paleo-plate reconstructions. Consequently, most mafic rocks exposed in the peri-Mediterranean Alpine Belt have been extensively studied especially in the Alps, Betic-Rif and Tyrrhenian sectors (e.g. Lustrino et al., 2011; Varas-Reus et al., 2018). Conversely, except for some pioneer studies (e.g. Bosch et al., 2014; Mechati et al., 2017), mafic/ultramafic occurrences in the Maghrebides of northern Algeria, have not been studied in great details.

* Corresponding author.
E-mail address: delphine.bosch@gm.univ-montp2.fr (D. Bosch).

The geodynamic evolution of the present-day Western Mediterranean results from a long series of events starting in the Middle Jurassic with opening of the Ligurian Ocean, the western branch of the Alpine Tethys, connected and not well differentiated from the Piedmontese/Penninic/Nevado Filabride Ocean (e.g. Michard et al., 2006). Since the Cretaceous/Eocene, the geodynamic evolution of this area can be broadly summarized as resulting from the interplay of various lithospheric plates and microplates (Africa, Eurasia, Iberia and Adria) with oceanic domains in between (Carminati et al., 2012; Handy et al., 2010; van Hinsbergen et al., 2014). Most of the today's architecture is testimony of the domino effects that affected these different lithospheric units. The most salient features are linked to the consumption by subduction of the Ligurian Ocean, which according to most authors was a two-stage process. The first subduction event occurred during the Cretaceous (~130–85 Ma) and was responsible for the SE-directed, intra-oceanic, partial subduction of this oceanic domain. The second subduction stage, known in the literature as the Apennine-Maghrebide Orogeny, involved the NW-directed subduction of the Ligurian/Piedmontese Ocean beneath the united Iberia/Eurasia continental paleomargin, including the *AlKaPeCa* terrane (Bouillin, 1986). After the collision of the western margin of AlKaPeCa with the paleo-European south-eastern margin (forming the Greater Iberia, including Sardinia-Corsica and the Balearic promontory too), the collisional stresses between Africa and Europe were transferred to a new ocean, to the east of the new continental margin. This new subduction system, with opposite subduction polarity compared to the previous subduction Alpine phase, is known in literature as the Mesogea or Ionian Ocean, interpreted alternatively as the westernmost branch of the Neotethys or the eastern branch of the Alpine Tethys. The initiation of this subduction is still debated and could have started as early as ~85 Ma ago (e.g. van Hinsbergen et al., 2014; Vignaroli et al., 2008) with a very slow convergence velocity between 80 Ma and 35 Ma (e.g. Faccenna et al., 2014) or later, between ~68–65 Ma (e.g. Dercourt et al., 1986; Stampfli et al., 1998), ~53–50 Ma (Lustrino et al., 2017), ~49–42 Ma (Brun and Faccenna, 2008; Lustrino et al., 2009) and ~33 Ma (Doglioni et al., 1997; Schettino and Turco, 2006). Back-arc extension due to slab retreat (Carminati et al., 1998) began ~30 Ma (e.g. Faccenna et al., 2014; Jolivet et al., 2008) causing the opening of the LPB associated to the counter clockwise rotation of the Corsica-Sardinia block (Gattacceca et al., 2007). Opening of the Algerian Basin, south of the LPB is assumed to have occurred later, during the late Burdigalian (e.g. Mauffret et al., 2004; Medaouri et al., 2014).

In this study we present an integrated geochemical study (major and trace element analyses, along with Pb-Sr-Nd and Hf isotopes) of amphibolites and metagabbros from the allochthonous Kef Lakhal Complex of the Edough Massif, one of the most important massif (~20 km^2) of mantle-derived rocks outcropping in northeastern Algeria. This geochemical study has complemented by $^{40}Ar/^{39}Ar$ geochronology performed on amphibole separates. The main aim of this study is two folds: 1) to constrain the nature, origin and metamorphic overprint of amphibolites from the Kef Lakhal complex; and 2) to compare these data with those already available for the Western Mediterranean area, in order to propose an integrated tectonomagmatic model.

2. Geodynamical and geological setting

The Edough massif in northeastern Algeria belongs to the Maghrebides, a collisional zone extending from Morocco to Algeria, which represents the southern segment of the Apennine-Maghrebide Belt (Fig. 1A). The Maghrebides are interpreted as resulting from the Cenozoic fragmentation of the European paleomargin and the drifting of the resulting fragments, the so-called *AlKaPeCa* (Alboran, Kabylia, Peloritani Mts. and Calabria) terranes of Bouillin (1986), some of which (such as the Lesser and Greater Kabylia) ultimately collided with the northern margin of Africa. This massif (Fig. 1B), displays a ~40 km long NE-SW oriented dome shape and has been interpreted as a Miocene metamorphic core complex (Caby et al., 2001). The core of the massif is made up of granitoid rocks, gneisses, and diatexites associated with high-grade metasediments that are structurally overlain by pelitic schists and on top, by outliers of Mesozoic metasediments. The latter represent sedimentation on the African passive margin (the Tellian units) and are caped by Oligocene to early Miocene sediments (the Numidian flysch nappe). A small peridotite body, the Sidi Mohamed peridotites (SM), first identified by Bossière et al. (1976) is assumed to represent a piece of sub-continental lithospheric mantle (Bosch et al., 2014) emplaced into the crustal units at ~18 Ma (Bruguier et al., 2009). In the northwestern part of the massif, from bottom to top, three distinct units can be described above the granitoid basement. These are: 1) a high-grade metamorphic unit (HGMU) formed by metasediments associated with felsic and mafic-ultramafic rocks (amphibolites and peridotites; Fernandez et al., 2016); 2) a strongly deformed mylonitic zone and; 3) the Kef Lakhal amphibolite unit.

The high-grade metamorphic unit (Fig. 1C) includes kyanite-sillimanite-andalusite-bearing metasediments, marbles and amphibolite lenses (Ahmed-Said and Leake, 1997) that have experienced a HP-HT metamorphism (with metamorphic peak at ~700–750 °C and 12–14 kbar; Caby et al., 2001). This unit constitutes the footwall of the Kef Lakhal amphibolite unit and has been interpreted as the metamorphosed Permo-Carboniferous African paleomargin (Fernandez et al., 2016).

A main mylonite zone delineates the high-grade metamorphic unit from the Kef Lakhal amphibolite massif above. This zone has been interpreted as a mélange zone and contains relics of Oligocene UHP units including diamond-bearing metamorphic rocks (Bruguier et al., 2017; Caby et al., 2014). These metamorphic rocks were accreted to the base of the overriding Kef Lakhal Complex during its exhumation and thrusting onto the African margin at 20.85 ± 0.34 Ma (Fernandez et al., 2016). Similar and younger $^{40}Ar/^{39}Ar$ ages, from 20.8 ± 0.9 Ma to 15.5 ± 0.2 Ma on amphibole and mica (Fernandez et al., 2016; Monié et al., 1992), were assigned to the ultimate stages of extensive tectonic linked to the fast exhumation and cooling of the Edough Massif as a metamorphic core complex.

The upper unit is composed by the ~800 m thick allochthonous Kef Lakhal amphibolite unit (~4× ~ 5 km in its largest dimensions), first studied by Ahmed Said and Leake et al. (1997), and later by Caby et al. (2001). Rocks of this unit are mainly constituted by layered and porphyroblastic amphibolites with minor metagabbros. The variable abundance of plagioclase and mafic minerals in the amphibolites has been interpreted by Caby et al. (2001) as an igneous layering suggesting gabbroic protoliths. The unit is truncated at its base by the mylonite zone described above and displays an upward metamorphic gradient. At its base, dehydration melting of amphibolites is evidenced by the occurrence of garnet-rutile-bearing leucosomes parallel to the main foliation and attributed to metamorphism under P-T conditions of ~770–835 °C and 10–13 kbar (Caby et al., 2001). Garnet and rutile-free leucosomes, secant to the main foliation in the amphibolites, have been also described and correspond to lower pressure partial melting products. Isotope analyses indicate an oceanic affinity for the amphibolites which have been related either to a back-arc basin environment or to a remnant of the Ligurian Ocean (Bosch et al., 2014; Laouar et al., 2002). However, the nature and origin of the mafic and ultramafic rocks from the northeastern part of Algeria have not been investigated in details in spite of its significance for models aimed at tackling the geodynamic reconstruction through time of the Western Mediterranean. The main unresolved issues concerning this unit are related to its age, its origin and geodynamic setting and its evolution through time.

3. Analytical techniques

Detailed analytical procedures used for major elements, trace elements, Sr-Nd-Pb-Hf isotopes and Ar—Ar geochronology are available in Supplementary File-S1.

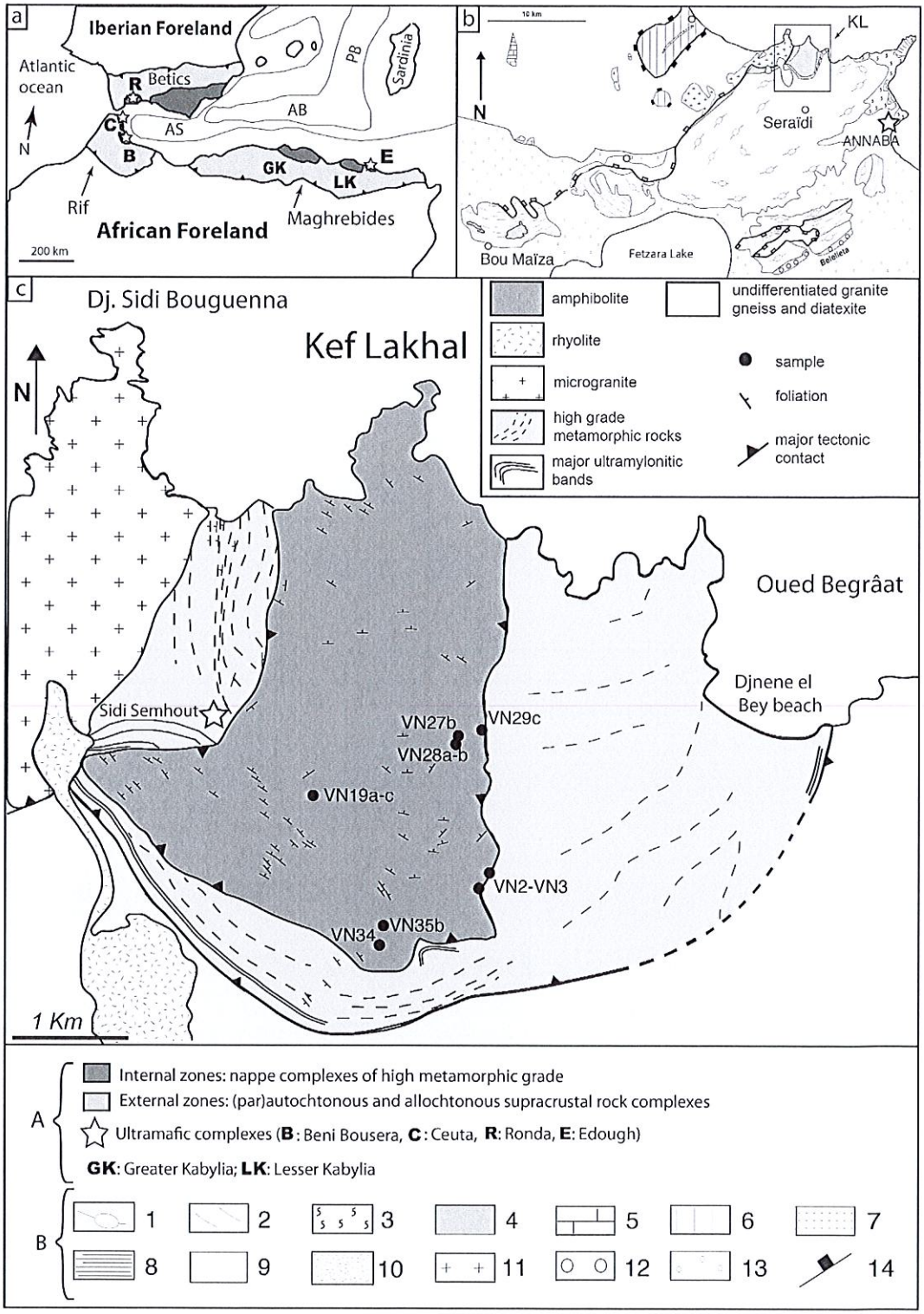

Fig. 1. A) Simplified tectonic framework of the Western Mediterranean area showing the main basins, major tectonic contacts and location of external and internal zones from the Peri-Mediterranean belts. Mantle outcrops are highlighted by light grey stars. Abbreviations as follow: Ronda (R); Ceuta (C); Beni Bousera (B); Greater Kabilia (GK); Lesser Kabylia (LK); Edough (E); Algerian Basin (AB); Alboran Sea (AS); Provencal Basin (PB) (modified after Bruguier et al., 2009). B) Geological sketch map of the Edough Massif (after Caby et al., 2001). 1 = granite-gneiss; 2 = micaschists; 3 = high-temperature metamorphic rocks; 4 = undifferentiated mafic and ultramafic rocks; 5 = Jurassic marbles; 6 = Cretaceous marls and flysch; 7 = Mesozoic phyllites; 8 = ultramylonites bands; 9 = Numidian nappe; 10 = Langhian rhyolite; 11 = microgranite; 12 = Pliocene sediments; 13 = Quaternary cover; 14 = major normal fault. Kef Lakhal is KL. C) Enlargement of the geological sketch map of the Kef Lakhal area in the Edough Massif from NE Algeria (modified after Caby et al., 2014; reported foliations are from Ahmed-Said and Leake, 1997).

4. Sampling

4.1. Field observations

On the field, the amphibolites occur either as banded rocks with alternating feldspar ± epidote-rich layers (leucocratic parts in Fig. 2a-c) and amphibole-rich layers (melanocratic parts in Fig. 2a–c) or as melanocratic massive benches. In the banded amphibolites, the epidote-rich layers constitute a weak proportion of the rock volume and were not sampled for this study. As shown in Fig. 2d some amphibolites show the macroscopic presence of melt pockets. Metagabbros appear as lenses enclosed in the massive amphibolites.

4.2. Petrography

Petrographic observations on rocks from the Kef Lakhal unit confirm field observations and reveal three main rock types: porphyroblastic amphibolite, banded amphibolite and metagabbro.

4.2.1. Porphyroblastic amphibolites (3 samples)

Porphyroblastic amphibolites (Fig. 3a–b) are mainly composed of amphibole (~70–85% vol.), feldspar (15–30% vol.), titanite (1–2% vol.), pyroxene (<1% vol.), accessory minerals (sulphides and oxides), and scarce epidote and apatite. Amphibole is mostly of hornblende-type. The brown to green pleochroic amphibole is often poikiloblastic for the abundant presence of apatite, epidote and/or rutile without clear specific orientation suggesting a magmatic origin. Plagioclase is well crystallized and shows sharp and clear rims with coexisting amphibole. In some parts, a fine-grained matrix composed of intermingled plagioclase and epidote is observed. Titanite is scarcely present, while garnet has been observed in one sample.

4.2.2. Banded amphibolites (5 samples)

Banded amphibolites display a repeated alternation of melanocratic and leucocratic layers (Fig. 3c–d). This type of sample mostly contains brown amphibole, plagioclase, titanite, ±clinopyroxene, ±garnet. Amphibole defines schistosity as in the previous types, and occasionally shows exsolution and reaction rims (VN2). Some corrosion gulfs containing titanite have also been observed (e.g. VN3). In general amphibole displays numerous accessory mineral inclusions such as titanite, apatite, and rare minute zircon. Plagioclase is present in two textural sites in melanocratic bands, either in equilibrium with amphibole or intermingled with finely grained epidote and quartz. Leucocratic bands mostly contain plagioclase and poikilitic epidote megacrysts. In some samples (e.g. VN19a), secondary epidote veins crosscut the main schistosity. Rare relics of clinopyroxene with irregular edges have been observed in few samples (VN2, VN3, VN29c; Fig. 4a–c). Deformed pockets composed of plagioclase ± quartz and displaying sigmoid shapes have been observed occasionally along the main foliation.

4.2.3. Metagabbros (2 samples)

Metagabbros (VN28b and VN34) are mainly composed of epidote, plagioclase and clinopyroxene relics (Figs. 3e–f and 4e). Some hornblende-rich bands have also been observed and are similar to those previously observed in porphyroblastic amphibolites. In the epidote-rich zone, plagioclase is euhedral whereas in hornblende-rich zone, plagioclase is intermingled with epidote. Hornblende is often rich in titanite inclusions and shows numerous exsolution along cleavages.

5. Results

5.1. Major elements on minerals

In situ major element analyses (EMP) on minerals are reported in Supplementary File S2, and the most relevant features are presented below.

Amphibole from porphyroblastic and banded amphibolites is overall similar, and in the $Mg/(Mg + Fe^{2+})$ vs Si discriminant diagram (Leake et al., 1997), corresponds to magnesio-hastingite (Fig. 5a). Amphibole from the banded amphibolite VN19a yields a different chemistry and plots in the magnesio-hornblende to tschermakite field (see Fig. 5b), similarly to amphibole from the metagabbro VN34. In the banded amphibolites and in the metagabbros, pyroxene is Mg—Fe and Ca rich (CaO = 21.9–25.1) and is mainly diopside ($En_{32-39}Fs_{09-17}Wo_{50-53}$) (Fig. 5c). Plagioclase displays variable anorthite contents ranging from intermediate to calcic ($An_{28-94}Ab_{71-06}Or_{0-1}$ and $An_{21-65}Ab_{77-34}Or_{0-2}$) in the

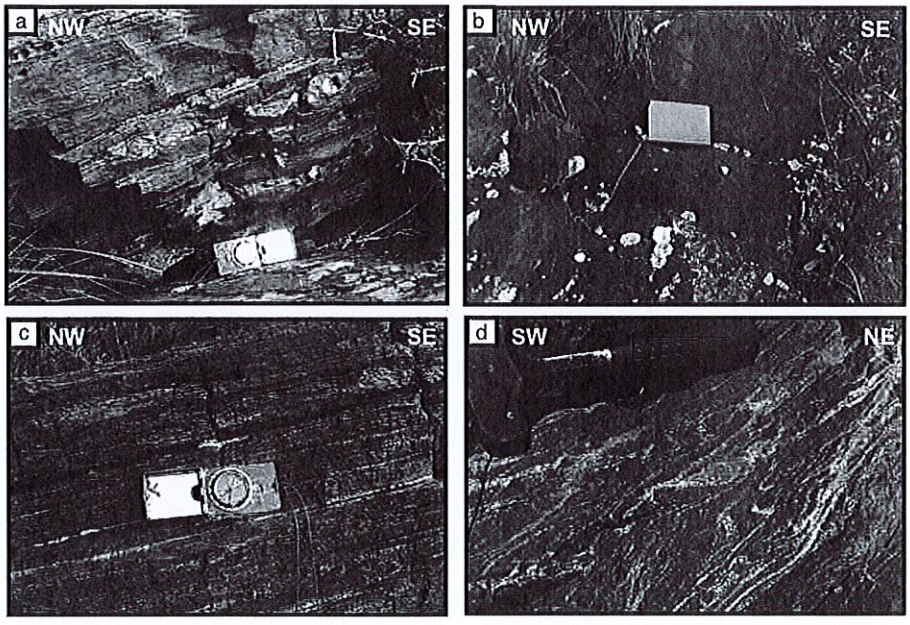

Fig. 2. Field pictures showing different types of amphibolites. a-b) Amphibolite from the top of the Kef Lakhal complex mainly composed of feldspar and amphibole and showing deformed epidote-rich levels. c) Amphibolite with plagioclase-rich levels. d) Traces of partial melting in this amphibolite.

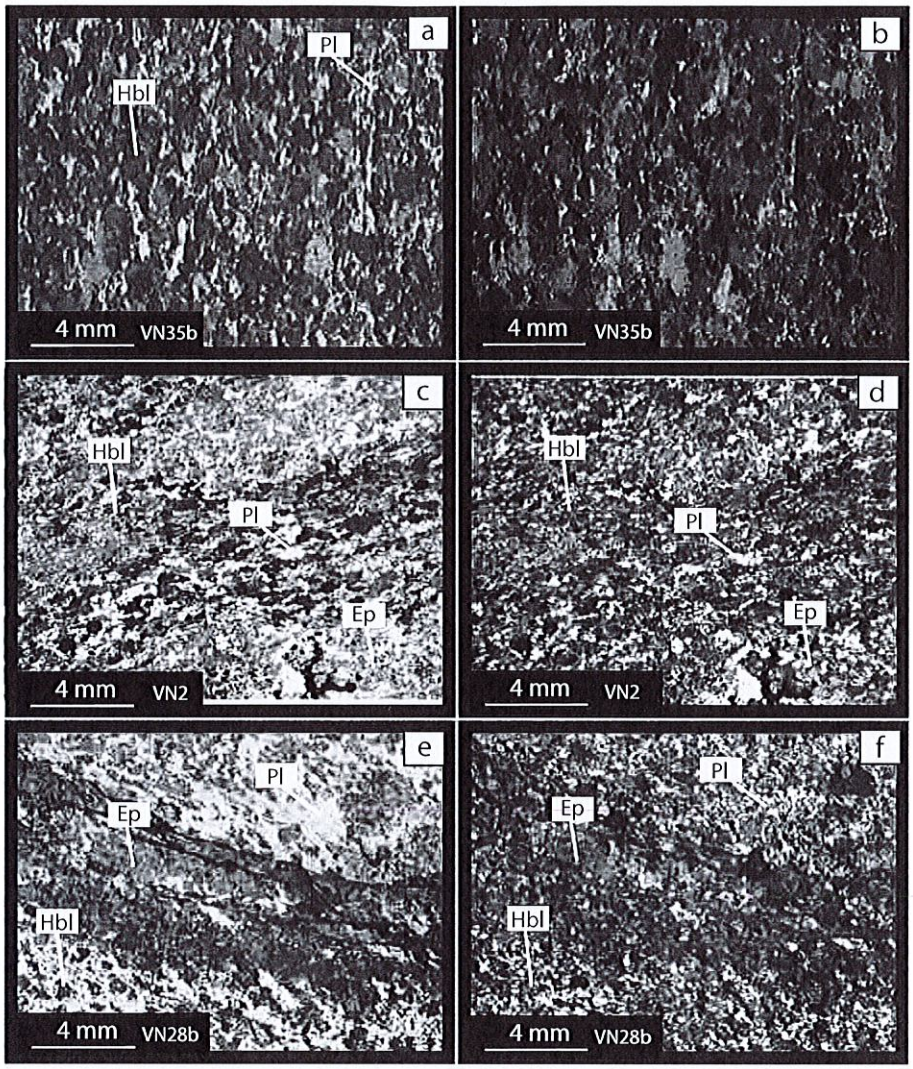

Fig. 3. Representative thin section microphotographs of Kef Lakhal amphibolites and metagabbros. a-b) amphibolite VN35b with hornblende porphyroblast and finely crystallized plagioclase and quartz; c-d) amphibolite VN6b with oxide-rich epidote levels; e-f) metagabbro VN28b rich in epidote, with some levels containing plagioclase, quartz and hornblende. Abbreviations are the followings: Pl: plagioclase, Ep: epidote, Hbl: hornblende.

porphyroblastic and banded amphibolites respectively which is consistent with the analysis of one plagioclase in the metagabbro VN28b ($An_{31}Ab_{68}Or_{01}$). Garnet is scarce and has been analysed only in the porphyroblastic amphibolite VN27b and in the banded amphibolite VN2. In both samples garnet is homogenous with no zonation from core to rim. It is rich in almandine ($X_{Alm} = 46–48$) and grossular ($X_{Grs} = 30–37$) components. In addition, in the porphyroblastic amphibolite VN27b, one garnet relic is richer in MgO ($Alm_{38}Grs_{22}Prp_{38}Spss_2$). Epidote is present in all samples and displays a high clinozoisite content of $C_{Zo}88–100$, $C_{Zo}72–84$, $C_{Zo}81–87$ for the porphyroblastic amphibolites, banded amphibolites and metagabbros respectively.

The garnet-amphibole-plagioclase barometer (Kohn and Spear, 1990) applied to amphibolites provides pressures between 7 and 10 kbar for both the porphyroblastic and banded amphibolites (for a temperature input of 800 °C). Plagioclase-amphibole thermometer (Holland and Blundy, 1994) yields, for most Kef Lakhal amphibolites, a temperature estimate ranging from ~700 °C to 800 °C (± 50 °C) in good agreement with those determined by Ahmed-Said and Leake (1997). The porphyroblastic amphibolite VN35b, yields temperatures of 837 ± 50 °C and 865 ± 50 °C (for 7 kbar and 10 kbar, respectively), slightly higher than those calculated for other samples.

5.2. Bulk rock major and trace elements

Results for major and trace elements on bulk rocks are available in Supplementary File S3. The amphibolites yield low mass loss on ignition (<1.96 wt%), variable Mg# number (48.8–64.5) and high TiO_2 content (>1.65%). There is a tendency for the porphyritic amphibolites to display Mg# (>59) higher than the banded amphibolites (<52). The two metagabbros exhibit major element composition similar to the amphibolites, but are characterized by lower MgO (<3.5 wt%), Na_2O (<1.6 wt%) and K_2O (<0.15 wt%), as well as higher CaO (~19 wt%). The Mg# values are too low to be representative of unfractionated melt compositions in equilibrium with a classical peridotitic matrix, indicating variable extents of fractional crystallisation. In the TAS diagram (Le Bas et al., 1986), the two types of amphibolites and the metagabbros show a basaltic composition except the porphyroblastic amphibolite VN35b and the banded amphibolite VN29c which both plot in the picro-basalt field (Fig. 6). In the classification diagram using immobile elements (Pearce, 1996), more appropriate for altered rocks, the scatter of the data point is reduced and the studied rocks are all clearly classified as tholeiitic basalts.

Amphibolites and metagabbros are characterized by overall similar primitive mantle-normalized incompatible element and chondrite-

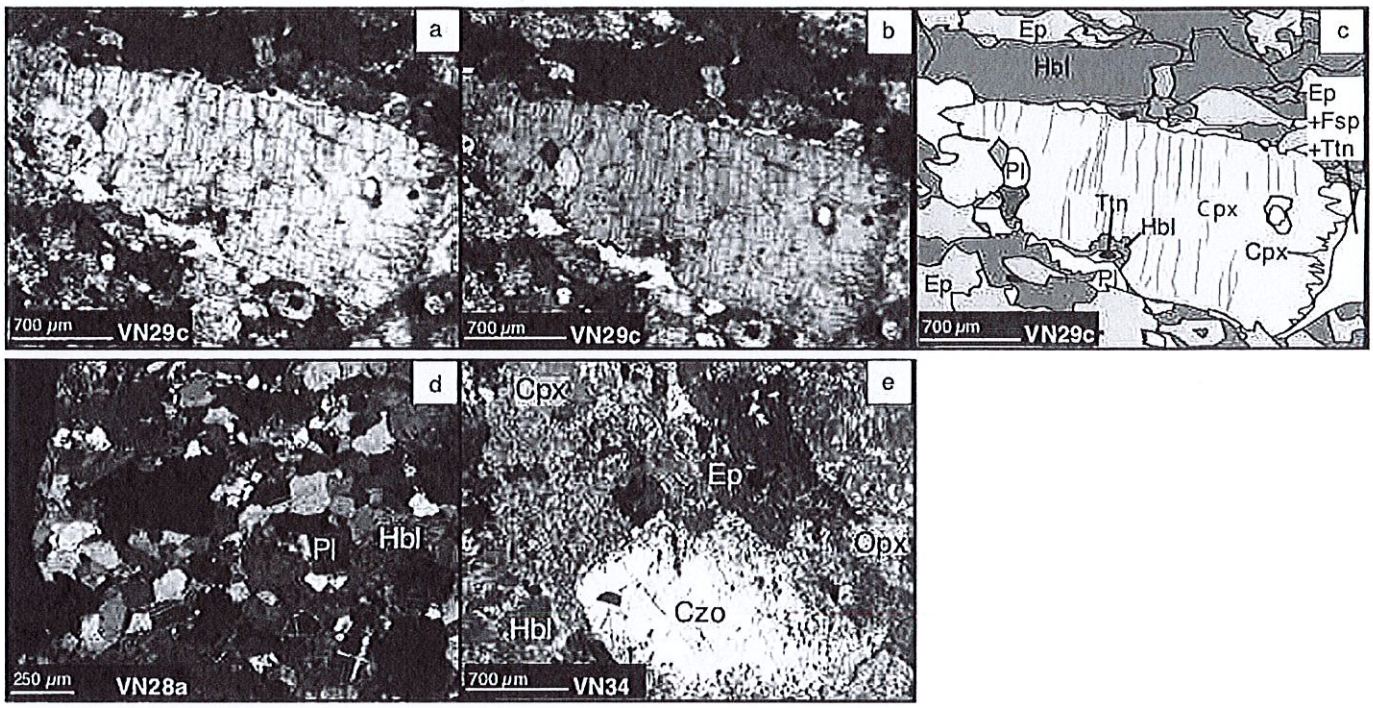

Fig. 4. Thin section microphotographs. a-c) Banded amphibolite showing a clinopyroxene relict; (d) Porphyroblastic amphibolite VN28a with clean boundary between plagioclase and hornblende; (e) Metagabbro VN34 showing a clinozoisite macrocrystal and a clinopyroxene destabilized in epidote. Abbreviations are the followings: Cpx: clinopyroxene, Opx orthopyroxene, Czo: clinozoisite, Ttn: titanite, Fsp: fedspar.

normalized REE patterns (Fig. 7). In the diagrams of Fig. 7, they are compared to N-MORB (black line, Sun and McDonough, 1989) and to Global MORB (thick red line, Arevalo and McDonough, 2010), the latter including a small proportion of *E*-MORB. Most studied samples yield REE patterns depleted in light (L) REE ($La/Sm_N < 1$) and in heavy (H) REE relative to medium (M) REE ($Sm/Yb_N \geq 1.4$), which is more comparable to Global MORB than to N-MORB. Exceptions are the two porphyroblastic amphibolites VN27b and VN28a which show a moderate upward slope to the left ($La/Sm_N = 1.1–1.2$), thus resembling E-MORB like patterns. Most samples have no Eu anomalies ($Eu/Eu^*_N = 0.9–1.0$) or a weak positive anomaly for the two porphyroblastic amphibolites VN27b and VN28a ($Eu/Eu^*_N = 1.2$ and 1.1 respectively) and the metagabbro VN28b ($Eu/Eu^*_N = 1.1$) suggesting the melts were little fractionated by plagioclase accumulation/removal. Compared to MORB (both Global and Normal), all samples show variable enrichments in Large Ion Lithophile Elements (LILE), notably Cs and Rb which can be up to 10–100 times primitive mantle estimate. Only metagabbros and one prophyroblastic amphibolite show Ba enrichment. In addition, the banded amphibolites and the metagabbros display positive U anomalies that are lacking in the porphyroblastic amphibolites. Strontium yields either positive (metagabbros) or negative (banded amphibolites) anomalies or both (porphyroblastic amphibolites). All samples are characterized by negative Pb anomalies, mimicking MORB, and by a slight Ti negative anomaly which is also present in the Global MORB but not in N-MORB. Other HFS elements (Zr, Hf, Nb and Ta) do not show significant anomalies, although the porphyroblastic amphibolite VN27b displays a Ta spike.

5.3. Ar-Ar geochronology

$^{40}Ar/^{39}Ar$ geochronology was performed on single crystals of amphibole from two banded (VN3 and VN19c) and one porphyroblastic (VN28a) amphibolite. $^{40}Ar/^{39}Ar$ plateau ages obtained on the three amphibolites show a very restricted range, from 18.03 ± 0.36 Ma (VN28a) to 18.90 ± 1.11 Ma (VN19c; Fig. 8a–c). Corresponding inverse isochrons are consistent within errors and range from 17.45 ± 0.50 Ma (VN28a) to 18.73 ± 2.21 Ma (VN3). In addition, they do not display excess argon contamination, all initial $^{40}Ar/^{36}Ar$ being close to the atmospheric value of 295.5 (Fig. 8a–c and Supplementary File S4). Considering that the amphibole plateau ages in the three studied samples are undistinguishable within errors, a weighted mean age (plateau ages) of 18.14 ± 0.27 Ma (MSWD = 1.2) has been calculated.

5.4. Sr, Nd, Hf and Pb isotopes

Isotopic ratios need to be corrected for in situ decay, but until now, no precise magmatic age is available for the Kef Lakhal Complex (the significance of the amphibole Ar age is discussed below). Considering the geodynamical context of the Western Mediterranean, we assume that the time interval 150–40 Ma corresponds to the most likely age range of the studied samples. Isotopic ratios (Supplementary File S5) were thus age-corrected at both 40 Ma (the age of the oldest subduction-related magmatic activity in the Western Mediterranean after Lustrino et al., 2009, 2017) and 150 Ma (the mean age of the Ligurian oceanic crust, e.g. Tribuzio et al., 2016). Data points appearing in the various isotope diagrams (Fig. 9) correspond to 40 Ma age-corrected values, and we have also indicated the field corresponding to 150 Ma corrected values. It is noteworthy that the discussion and interpretations below remain valid regardless of the true age of the samples as long as it stands within this range.

The porphyroblastic amphibolites and the coexisting minerals show limited but significant variations in age-corrected Sr isotopic ratios with values ranging from 0.70322 to 0.70429 (Supplementary File S5). Nd isotopic ratios range from 0.51287 to 0.51306, where the lowest value is from the amphibole fraction of sample VN28a. On a Nd—Sr isotopic diagram (Fig. 9a), samples plot close to the DMM end-member and overlap the MORB field except sample VN35b, which yields a higher $^{87}Sr/^{86}Sr$ ratio of 0.70429 (Supplementary File S5). The banded amphibolites and coexisting minerals show Sr isotopic ratios higher and more variable than the porphyroblastic amphibolites. $^{87}Sr/^{86}Sr$ ratios

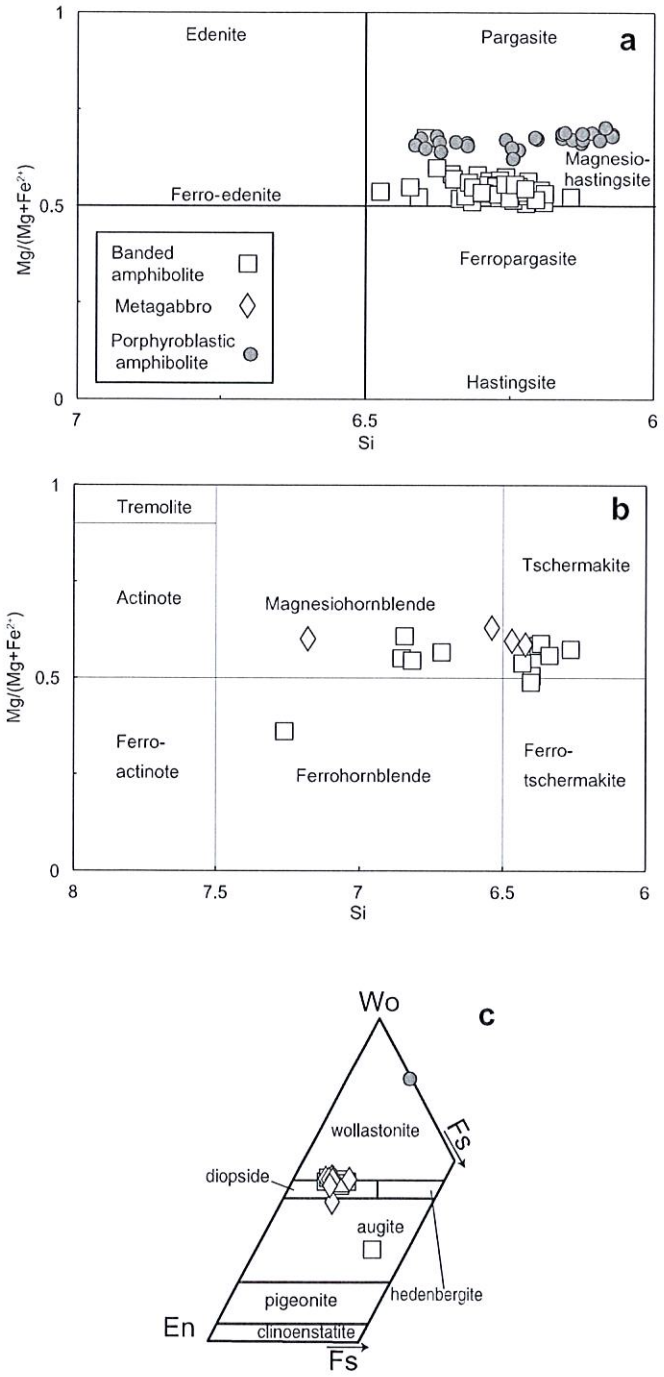

Fig. 5. Discriminant diagrams for amphibole after Leake et al. (1997) calculated in atom per formula unit. a) Calcic amphibole with: $Ca_B > 1.50$; $(Na + K)_A > 0.50$; $Ti < 0.50$. b) For calcic amphibole satisfying the following criteria: $Ca_B \geq 1.50$; $(Na + K)_A < 0.50$; $Ca_A < 0.50$. c) Ternary diagram for major elements in situ analyses of pyroxene (Morimoto, 1988). Abbreviations: (Wo) Wollastonite, (En) Enstatite, (Fs) Forsterite.

(0.70313–0.70856) range from DMM to more radiogenic compositions tending towards seawater composition (i.e. 0.70916 for present-day seawater; Palmer and Edmond, 1989), where the highest value is from the amphibole fraction of sample VN19c. Nd isotopes are typical of a DMM end-member and range from 0.51304 to 0.51310. On the Sr—Nd isotopic diagram (Fig. 9a), whole-rock and mineral data plot close to the DMM end-member and, except amphibole VN28a and VN27b, define a horizontal array parallel to the x-axis. Only one metagabbro (whole-rock and minerals separates) was analysed for Sr and Nd isotopes. The results are consistent with those obtained on the banded amphibolites with Sr and Nd isotopic compositions ranging from 0.70366 to 0.70537 and from 0.51302 to 0.51310 respectively.

The amphibolites (porphyroblastic and banded) and the metagabbro VN28b yield a very limited range of Hf isotopic values, ranging from 0.28303 to 0.28315 with the exception of the amphibole fraction from the porphyritic amphibolite VN28a, which yields a significantly lower $^{176}Hf/^{177}Hf$ isotopic composition of 0.28276. It is noteworthy that this enriched Hf isotopic signature is also reproduced by the Nd composition (0.51287), whereas the Sr isotopic composition is amongst the lowest of our dataset (0.70322). Reported in the Hf—Nd isotopic diagram (Fig. 9b) samples plot close to - but slightly below to - the Nd—Hf mantle array. With the exception of the amphibole fraction of sample VN28a, all separated minerals yield isotopic ratios close to or similar to those of the associated whole-rocks (Supplementary File S5).

As concerns Pb isotopic ratios (Fig. 9c–d) the studied samples and their minerals yield a limited range of variation of the $^{206}Pb/^{204}Pb$ ratios, ranging from 18.41 to 18.74 (Supplementary File S5). On the other hand, the $^{207}Pb/^{204}Pb$ and $^{208}Pb/^{204}Pb$ ratios display a larger variability (from 15.49 to 15.59 and from 37.73 to 38.42, respectively). In Fig. 9c–d, these features result in a broadly vertical distribution, spreading between the DMM domain and the field of subducted and marine sediments, including EM2 and GLOSS (Global Subducting Sediments, Plank and Langmuir, 1998) end-members, but the data remain in the MORB field.

In summary, the Kef Lakhal samples show a clear decoupling between Sr, Nd, Hf and Pb isotopes. Nd and Hf isotopic signatures are close to DMM with participation of a seawater component detected only on the Sr isotopic signature of some samples. Pb isotopes show participation of a more evolved component with isotopic characteristics trending towards a EM2 or GLOSS component.

6. Discussion

6.1. Timing of metamorphic evolution

Using the plagioclase-amphibole thermometer of Holland and Blundy (1994) a temperature range of 700–865 °C is calculated for the studied amphibolites. This temperature range concurs with previous studies (e.g. Caby et al., 2001) on amphibolites from the Kef Lakhal unit which provided P-T conditions of 770–835 °C and 10–13 kbar for the climax of the metamorphic overprint. This temperature range is well above the admitted closure temperature for Ar in amphibole (550 ± 50 °C after Dahl, 1996) and the 18.14 ± 0.27 Ma weighted mean amphibole age is thus confidently taken as an average metamorphic age through the amphibole closing temperature. It is noteworthy that this age is similar to those obtained on amphibole from amphibolites sampled within the mélange zone below the Kef Lakhal unit (samples VN14a and VN16d of Fernandez et al., 2016) which cluster in the 18–19 Ma age range. The similarity in Ar amphibole ages in the Kef Lakhal unit and in the metamorphic sole below on one hand, and with U—Pb monazite ages (17.84 ± 0.12 Ma) in the core of the Edough Massif (Bruguier et al., 2009) on the other hand indicates a similar fast cooling history and substantiates that the metamorphic pile of the Edough Massif was exhumed as a whole during the Burdigalian. This lends support to the conclusion reached by Fernandez et al. (2016) that the Kef Lakhal amphibolite unit was thrust onto the crustal units of the Edough massif at ~21 Ma, before to underwent a common cooling history during exhumation of the massif as a metamorphic core complex.

6.2. Element mobility in the Kef Lakhal amphibolitic unit

Previous studies have demonstrated the imprint of a Miocene metamorphic event in the whole Edough Massif (e.g. Bruguier et al., 2009, 2017; Fernandez et al., 2016; Monié et al., 1992), which is consistent with the Ar amphibole ages obtained during the course of this study.

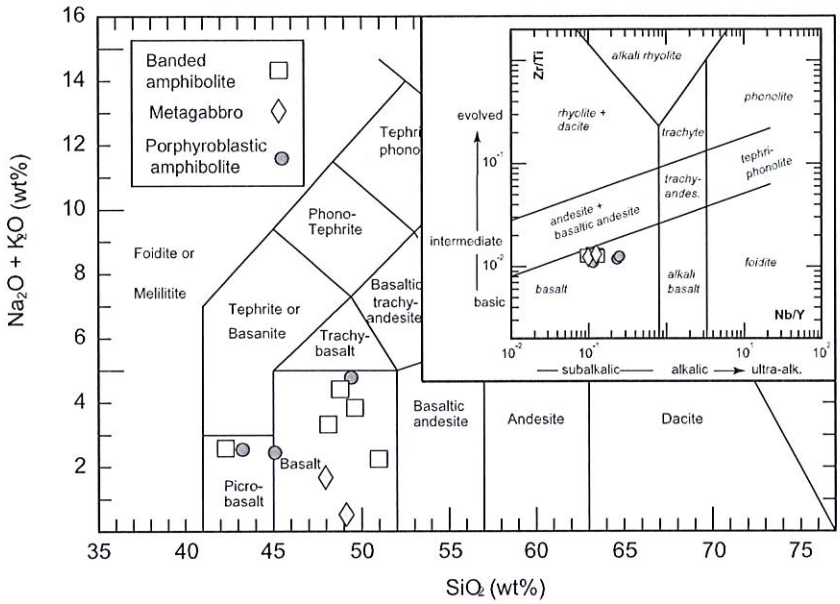

Fig. 6. TAS (Total Alkali Silica) diagram after Le Bas et al. (1986) and Zr/Ti vs. Nb/Y discrimination diagram for immobile elements of Pearce (1996).

Before to discuss the sources of the Kef Lakhal amphibolites, it is thus necessary to examine the possible effects of such events on the chemical and isotopic signature of the studied rocks in order to emphasise which characteristics are source-related and which are related to latter events (alteration/metamorphism).

The most striking features of primitive mantle-normalized multi-elemental diagrams (Fig. 7) are a clear increase in alkalis (Cs and Rb), which is present in all studied samples, and positive U anomalies, not observed in the porphyroblastic amphibolites, which indicate significant U uptake. During hydrothermal alteration, the upper oceanic crust is a sink for Rb, Cs and U (e.g. Staudigel et al., 1989), which can be added to the crust during exchange with seawater at low temperature and up to lower greenschist facies conditions (Bach et al., 2003). In a study of altered oceanic crust at ODP site 801, Kelley et al. (2003) demonstrated that the largest effect of seafloor alteration is to increase the alkalis and U, associated with little or no enrichments in Ba or Pb. This is consistent with our results, which, similarly to N- and Global-MORB patterns, display negative Pb anomalies in primitive mantle-normalized diagrams. On the contrary, the clear enrichment of Ba in the metagabbros and in the porphyroblastic amphibolite VN28a is not observed in the banded amphibolites nor in the porphyroblastic amphibolites VN27b and VN35b. It seems, therefore, that enrichments in Cs, Rb, and U ($\pm$ Ba) recorded in primitive mantle-normalized diagrams can be related to oceanic crust–seawater interaction and alteration. The observation that positive U anomalies are lacking in the porphyritic amphibolites is consistent with a less intense alteration in massive rocks.

Plagioclase from the amphibolites (porphyroblastic and banded) shows overall a variable anorthite content, broadly ranging from oligoclase ($An_{21}Ab_{77}Or_{02}$) to anorthite ($An_{94}Ab_{06}Or_{00}$). The extent of variation in the composition of plagioclase is likely to reflect various degrees of alteration. The low anorthite content of some plagioclase crystals is related to metamorphism or to seawater interaction and hydrothermal alteration during which Ca-rich plagioclase is converted to albite and laumontite first and then albite and epidote in the greenschist facies (Humphris and Thompson, 1978).

The replacement of the original plagioclase (the main Sr host in basaltic rocks) by albite during seawater interaction is consistent with Sr isotope results. The Sr isotope data show that four out of six bulk rock analyses (Supplementary File S5) have $^{87}Sr/^{86}Sr$ ratios lower than 0.7045 (0.70355–0.70432), which, although distinct from typical MORB (0.70282; Gale et al., 2013), are considerably lower than the present-day seawater value (0.70916; Palmer and Edmond, 1989). These overall low values are correlated with data from mineral separates (amphibole, clinopyroxene and plagioclase) which yield similar Sr isotope compositions to their host rocks (0.70333–0.70439). However, it is worth noting that amphibole separates overall tend to have the highest Sr isotope compositions. In particular, the amphibole separate from VN19c has a $^{87}Sr/^{86}Sr$ (0.70894) very close to present day seawater. Following the recently revised Sr seawater evolution curve of Wierzborwski et al. (2017), such a high $^{87}Sr/^{86}Sr$ seawater value has never been reached during the whole Jurassic (maximum $^{87}Sr/^{86}Sr$ = 0.70732 during the Early Jurassic) but corresponds to the early Miocene (Palmer and Edmond, 1989). This indicates that relatively recent alteration by seawater or by seawater-derived fluids has likely affected this sample. The moderate increase in Sr isotope composition of most bulk rocks, along with the low $^{87}Sr/^{86}Sr$ of mineral separates, indicates however that such alteration did not pervasively modify the Sr isotopic composition of the studied samples and/or that the leaching procedure performed on the bulk rocks and mineral separates (see Supplementary File S1) efficiently removed alteration phases. This in turn suggests that seawater alteration is likely to be stored only in alteration phases formed in equilibrium with seawater, such as albite replacing plagioclase, or epidote which, although avoided during sampling is present in all studied samples. The occurrence of epidote is known to enhance Sr content in whole-rock analyses (e.g. Humphris and Thompson, 1978) and is likely to modify the original Sr isotopic composition. Consequently, Sr isotopes will not be considered further as a pristine source characteristic although most data appear rooted in the MORB domain in Fig. 9a.

It is important to assess whether the Pb isotopic signature is a source signal, or alternatively, whether it has been overprinted by alteration and/or metamorphism. The question is worth asking since Pb is classically considered as a fluid-mobile element and, as such, it can be subject to modifications due to its mobility in hydrothermal systems or during metamorphism. In addition, the U uptake, as seen in Fig. 7, can also be responsible for a modification of the $^{238}U/^{204}Pb$ ratio, thus leading to overcorrection of the age-corrected $^{206,207}Pb/^{204}Pb$ values. Lastly, in case of ancient uptake of seawater-derived U, the Pb isotopic composition can be significantly modified due to radiogenic ingrowth (e.g. Hauff et al., 2003). The Ce/Pb ratios of the studied samples (ranging

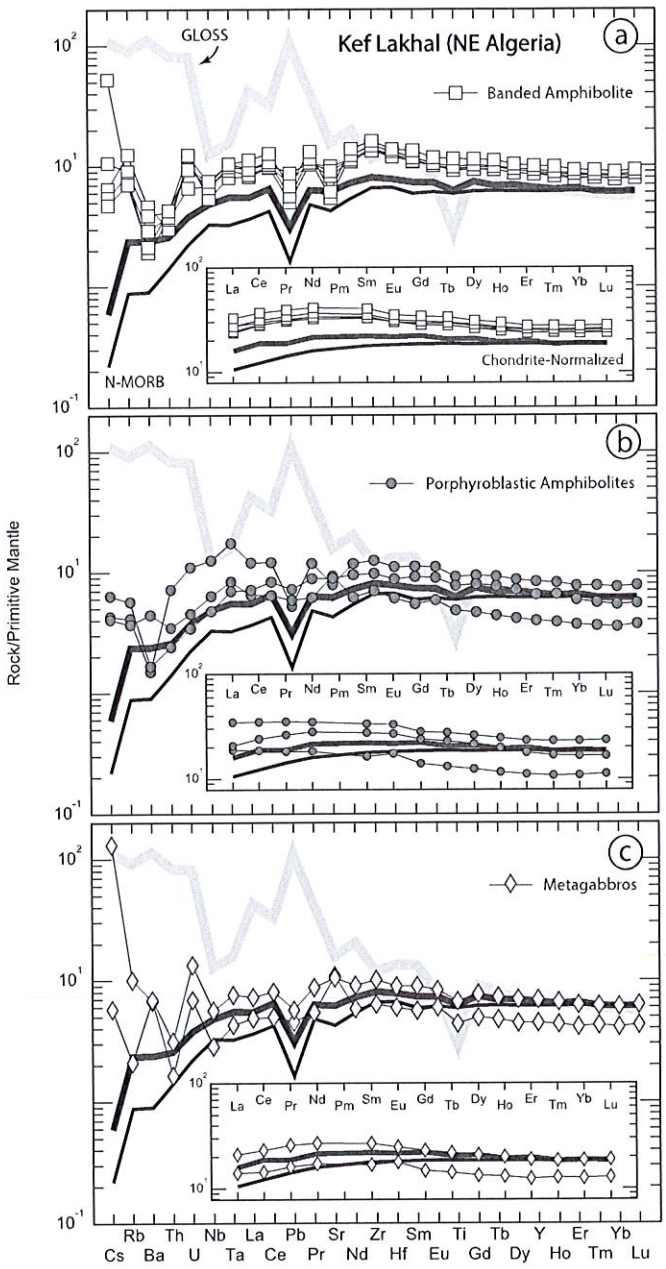

Fig. 7. Primitive mantle-normalized multi-elemental and chondrite-normalized REE diagrams for Kef Lakhal amphibolites and metagabbros. The thick red line is Global MORB (Arevalo and McDonough, 2010). N-MORB (plain black line) and normalization values (Primitive Mantle and Chondrite) are from Sun and McDonough (1989). (For interpretation of the references to colour in this figure legend, the reader is referred to the web version of this article.)

from 10.5 to 22.2; Supplementary File S3), are lower than, or within the range of the Ce/Pb of MORB (22.2 ± 9.7 after Arevalo and McDonough, 2010). The tendentially lower Ce/Pb ratios are attributed to an increase in Pb rather than to a Ce loss because REE patterns do not show any negative Ce anomalies and because the average Pb content of the studied samples (1.2 ppm) is twice higher than that of MORB (0.57 ppm; Arevalo and McDonough, 2010; Gale et al., 2013), whereas the mean Ce content (16.6 ppm) is close to that of the MORB (11.5–14.9 ppm; Arevalo and McDonough, 2010; Gale et al., 2013). We contend that the Pb isotopic values of the studied rocks can be considered as a source signal because: (1) the measured and age-corrected Pb isotopic values of all samples and their host minerals plot in the MORB field; (2) there is no detectable fractionation between uranogenic and thorogenic Pb which would have indicated an ancient U enrichment and a noticeable modification of the Pb isotopic values (e.g. Pettke et al., 2018), and (3) contrarily to Sr, the Pb concentration in seawater (~3×10^{-6} ppm after Kelly et al., 2009) is far too low to induce significant modifications of the Pb content and isotopic values of the studied samples.

On the basis of petrographic and geochemical data obtained from this study, i.e. witnesses of magmatic stages such as remnants of clinopyroxene, calcic plagioclase, low K_2O contents and a MORB-type signature (REE and Hf-Nd-Pb isotopes), we consider that the Kef Lakhal samples represent a fragment of altered oceanic crust that has not been thoroughly modified by post-crystallisation events and that preserve the source signature of their protolith. Fluid mobile elements, notably Cs, Rb and U (± Ba), display enrichments indicating that they do not reflect source characteristics but fluid-rock interactions. Sr isotopes also clearly show an interaction with seawater-derived fluids.

6.3. Nature of the protolith of the amphibolites

The previous section indicates that fluid-immobile elements (e.g. REE, HFSE) and the corresponding isotope ratios ($^{143}Nd/^{144}Nd$ and $^{176}Hf/^{177}Hf$) can be confidently regarded as indicators of source characteristics of the Kef Lahkal amphibolites. In addition Pb isotopes are also regarded as a feature relevant of the mantle source region.

Ti/Eu and Y/Ho ratios vary little during MORB genesis (melting, mixing and crystallisation) and consequently can be used as indicators of the mantle source region. In Kef Lakhal amphibolites, Ti/Eu ratios range from 6391 to 7569 and Y/Ho ratios from 27.4 to 29.0. These ratios perfectly lie within the range of variations of MORB (Ti/Eu = 7060 ± 1270, Y/Ho = 28.4 ± 3.6; Arevalo and McDonough, 2010) and strongly argue for a DMM source. Metagabbros display lower Ti/Eu ratios (5703 and 6251) but comparable Y/Ho ratios (28.5 and 28.9) that are still very consistent with a DMM source. Trace element discriminant diagrams (Pearce, 2008; Wood, 1980) further emphasise the MORB signature of the Kef Lakhal samples. In the discrimination diagram of Pearce (2008) all samples plot in the oceanic mantle array and the two samples with E-MORB-like REE patterns (VN27b and VN28a) plot close to the E-MORB end-member (Fig. 10a). This is further supported by the Th-Hf/3-Ta discrimination diagram (Wood, 1980) where these two porphyroblastic amphibolites plot in the E-MORB field (Fig. 10b), thus confirming the occurrence of both N- and E-MORB in the Kef Lakhal Complex. The occurrence of enriched MORB does not necessarily imply the proximity of a plume, since, as already noted by Gale et al. (2013), E-MORB are not always spatially associated with plume as can be observed along present-day ridge segments of the Pacific, Atlantic and Indian Oceans. Contrarily to Y/Ho and Ti/Eu, the Ce/Pb ratio, the third canonical ratio, is clearly out of the range of MORB for most samples (10.5–22.2). Considering that Ce and Pb do not fractionate sensibly during DMM source melting and MORB crystallisation, the low Ce/Pb ratios are taken as a feature of the depleted mantle source that melted to produce the Kef Lakhal samples. In the isotopic Pb diagrams of Fig. 9c–d, the Kef Lakhal whole-rock and mineral data points show a tendency suggesting that Pb isotopes are controlled by a two-component mixing where the enriched component is consistent with a sedimentary pole. However, lowering of the Ce/Pb ratio is also consistent with contamination by the continental crust (values of ~3.9 for the bulk continental crust; Rudnick and Gao, 2014) or by sediments derived therefrom.

The Ta/Hf vs Ho/Th diagram (Fig. 11a) was proposed by Niu and Batiza (1997) to discriminate between contamination by the continental crust or by recycled altered oceanic crust and sediments. In this diagram, melts issued from the different mantle reservoirs (OIB, E-MORB, N-MORB, Pacific MORB, Indian MORB, Atlantic MORB, Global MORB and ALL MORB) define an hyperbolic mixing curve between N-MORB and OIB, whereas the bulk (BCC) and Upper (UCC) continental crust (Rudnick and Gao, 2014) and GLOSS (Plank and Langmuir, 1998), which is dominated by terrigenous material of upper continental crust

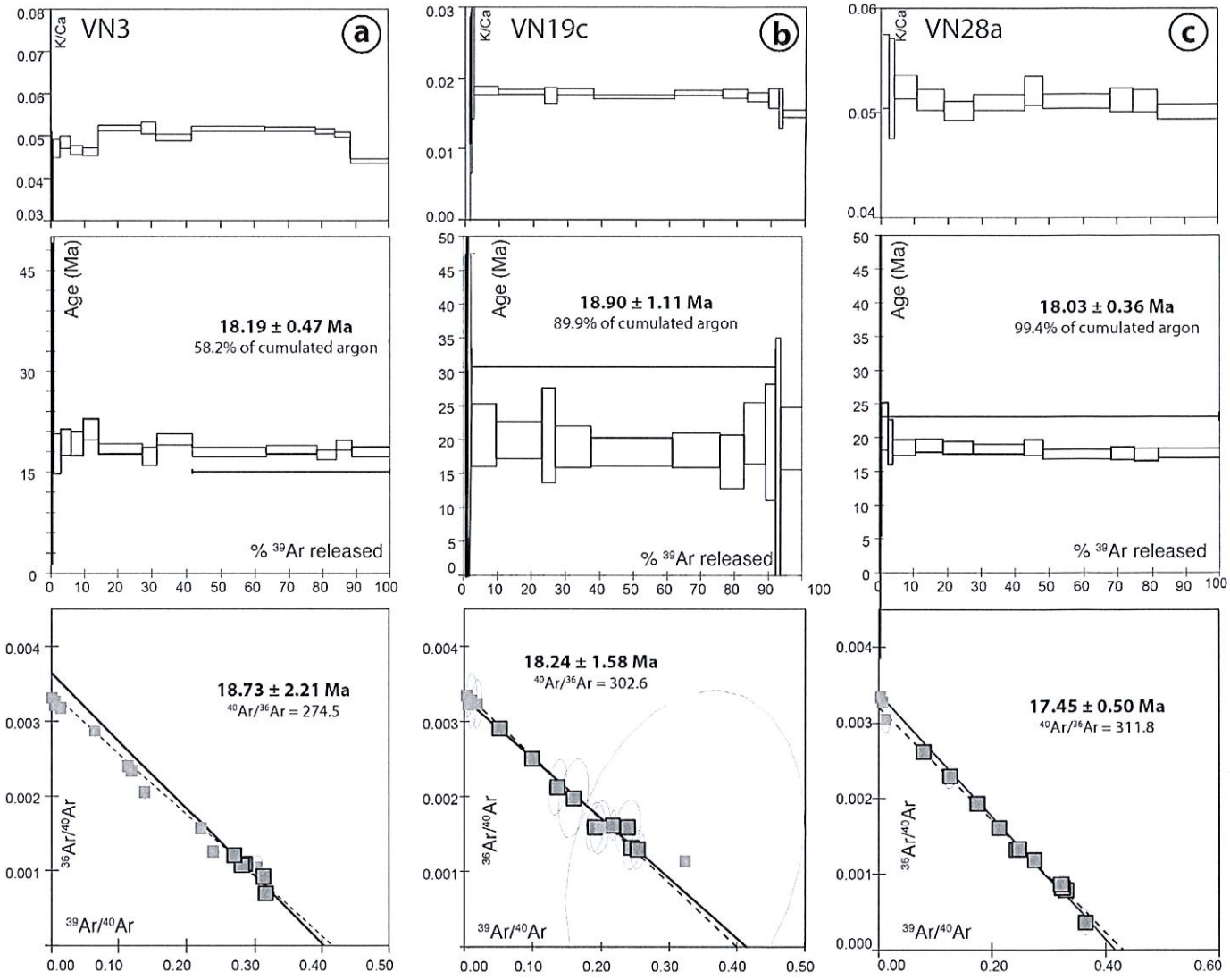

Fig. 8. K/Ca ratio, $^{39}Ar/^{40}Ar$ plateau ages and associated inverse isochrons obtained on separated amphibole from banded amphibolite (VN3 and VN19c) and porphyroblastic amphibolite (VN28a). Error margins are $\pm 2\sigma$.

origin, clearly plot on the left of the mixing curve. All the analysed Kef Lakhal whole rock samples plot mostly along such hyperbolic curve, thus ruling out contamination by the continental crust or by sediments with a high proportion of continentally-derived material. Consistently, terrigenous Paleozoic sediments from the underlying high-grade metamorphic unit of the Edough Massif (HGMU in Fig. 11a, after Fernandez et al., 2016), plot off the hyperbolic curve and locate very close to the bulk and upper continental crust.

Interestingly, sediments from the Mariana trench (ODP sites 800 and 801, Plank and Langmuir, 1998), which are dominated by volcaniclastic sources, plot above OIB, along the hyperbolic curve. This may suggest that such kind of sedimentary material is a likely end-member for contamination of the mantle source of the Kef Lakhal MORB-like melts. To gain insight into this process, we used the $^{206}Pb/^{204}Pb$ vs Ce/Pb diagram proposed by Klein and Karsten (1995) to distinguish between recently or anciently (relative to the genesis of the MORB melts) introduced contaminant to the mantle source. In such a diagram, lowering of the Ce/Pb ratios is accompanied by an increase of the $^{206}Pb/^{204}Pb$ ratios, which, due to radiogenic ingrowth can reach high values in the case of anciently recycled sediments. In Fig. 11b, the slight increase in $^{206}Pb/^{204}Pb$ isotope ratios accompanying a lowering of the Ce/Pb ratios, is not consistent with contamination by anciently subducted sediments in the mantle source. Recycling of upper Paleozoic (280–300 Ma) sediments from the underlying HGMU corresponding to the Paleozoic African passive margin is thus ruled out, inasmuch as these sediments have 1.6–1.9 Ga old Nd model ages indicating Meso- to Paleo-Proterozoic sedimentary precursors (Fernandez et al., 2016). On the contrary, the correlation roughly fits with contamination by recent sediments, with all samples being broadly aligned between MORB and present-day subducting sediments (GLOSS after Plank and Langmuir, 1998) including the Mariana's Trench sediments. The mantle sampled by the Kef Lakhal amphibolites and metagabbros was thus contaminated by a sedimentary component, probably dominated by volcaniclastic material. This sedimentary component was subducted shortly before magmatism and mixed to the ambient mantle prior to or during the melting event. Variations observed in the Pb isotopic diagrams (Fig. 9c–d) are attributed to varying proportions of this recycled component in the melting products. If so, one possibility is that the sedimentary component was not homogeneously distributed in the mantle source and hence has not been efficiently stirred by mantle circulation. The most likely explanation is then that this component remained in the depleted upper mantle where it has been mixed into the DMM matrix by convective processes. Since Nd and Hf systematics of the Kef Lakhal rocks preserve a DMM-like signature, we also argue that the

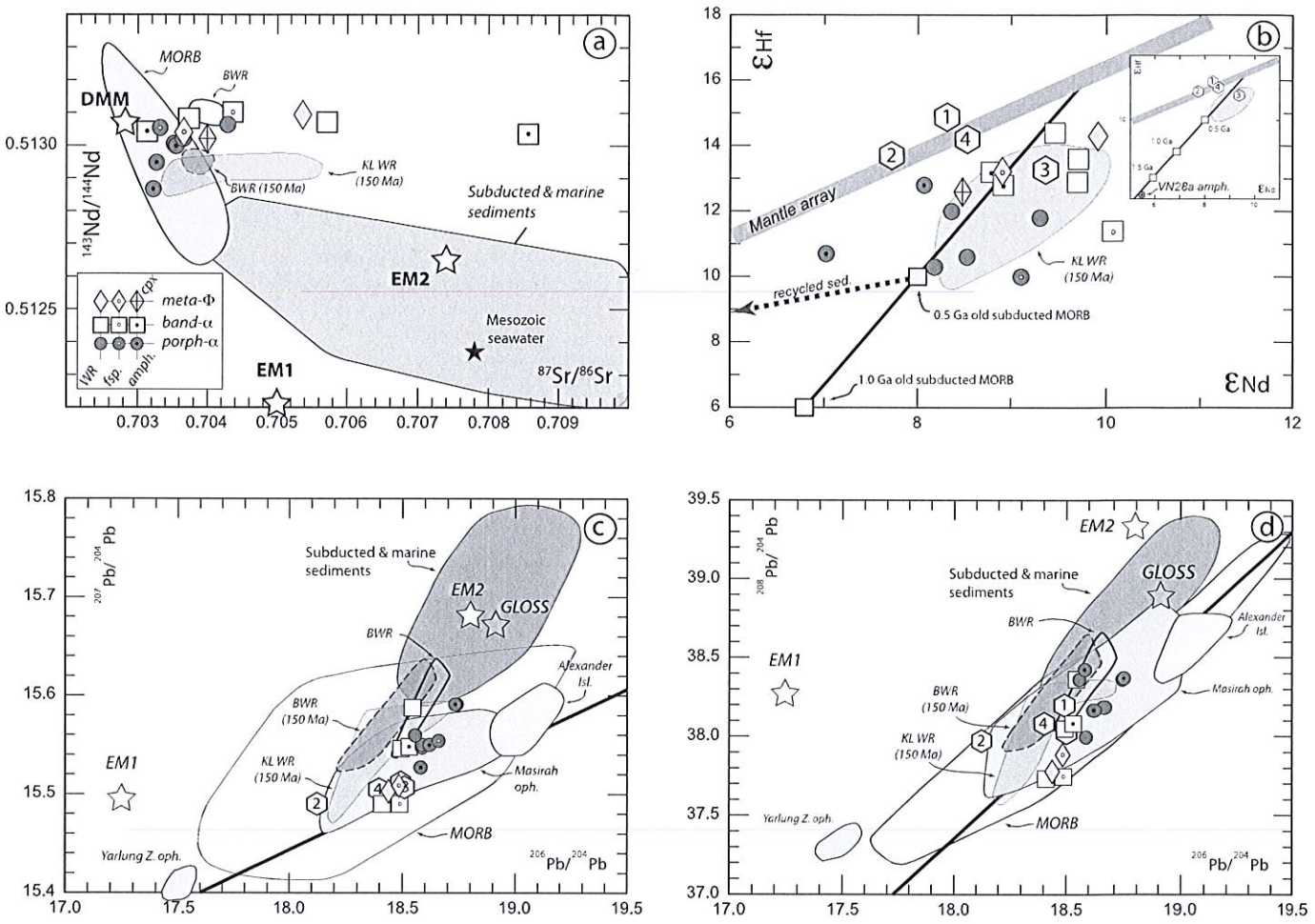

Fig. 9. Initial Sr-Nd-Hf-Pb isotope correlation diagrams for Kef Lakhal amphibolites and metagabbros. The field KL WR 150 refers to the isotopic ratios corrected for $t = 150$ Ma (Kef Lakhal Whole-rock 150 Ma). The fields BWR and BWR (150 Ma) refer to Kef Lakhal whole-rock analyses quoted in Bosch et al. (2014), age-corrected at 40 Ma and 150 Ma, respectively. (a) $^{143}Nd/^{144}Nd$ vs $^{87}Sr/^{86}Sr$ diagram; (b) $^{176}Hf/^{177}Hf$ vs $^{143}Nd/^{144}Nd$ diagram. The mantle array ($\varepsilon Hf = 1.33 \times \varepsilon Nd + 3.19$) is from Vervoort et al. (1999). Old recycled oceanic crust (yellow squares) and associated sediments (grey dashed arrow) are from Geldmacher et al. (2011); (c) $^{207}Pb/^{204}Pb$ vs $^{206}Pb/^{204}Pb$ diagram; (d) $^{208}Pb/^{204}Pb$ vs $^{206}Pb/^{204}Pb$ diagram. Reported for comparison are: subducted and marine sediments (Ben Othman et al., 1989; Plank and Langmuir, 1998; Vervoort et al., 2011). DMM (Depleted MORB Mantle; Workman and Hart, 2005), EM1, and EM2 (Enriched Mantle Type-1 and Type-2; Hart, 1988), and GLOSS (Global Subducting Sediments; Plank and Langmuir, 1998). MORB field from Georoc database http://georoc.mpch-mainz.gwdg.de/georoc/. Fields for Yarlung Zangpo ophiolite (Southern Tibet), Masirah ophiolite (Oman) and Alexander Island ophiolite (Antarctica) are from Mahoney et al. (1998). Symbols as follow: squares, grey circles, and grey diamonds are bulk rock analyses for banded amphibolites, porphyroblastic amphibolites and metagabbros respectively. Black dot, white dot and cross within symbols indicate mineral fraction analyses for amphibole, feldspar and pyroxene respectively. Empty hexagons labelled 1, 2, 3 and 4 are Atlantic, Pacific, Indian (White and Klein, 2014) and Global (Arevalo and McDonough, 2010) MORB. (For interpretation of the references to colour in this figure legend, the reader is referred to the web version of this article.)

proportions of the recycled sedimentary component were very small and probably mainly added to the MORB melts as a fluid component in which Pb can preferentially partition.

The Kef Lakhal samples are compared to the mean of the three present-day oceanic basins and global MORB (White and Klein, 2014), along with various occurrences of Tethyan MORB (Mahoney et al., 1998; Figs. 9b–d, 12). The Pb and Nd isotope signatures of the Kef Lakhal samples (Figs. 9c–d, 12) define a domain that includes the Pacific, Atlantic and Global MORB, whereas the Indian MORB are significantly offset to lower $^{206}Pb/^{204}Pb$ ratios. Similarly the field defined by the Masirah Tethyan ophiolite, which displays an affinity with the Pacific and Atlantic MORBs (Mahoney et al., 1998), overlap the Kef Lakhal domain, whereas the Yarlung-Zangpo ophiolite, with an Indian mantle signature, is clearly different. The lower $^{206}Pb/^{204}Pb$ ratios of the Indian Ocean MORB have been attributed to the recycling of anciently subducted oceanic crust and sediments (Rehkamper and Hofmann, 1997; Xu and Castillo, 2004). The distinction between the Kef Lakhal samples and the Indian MORB is therefore consistent with a short residence time for the sedimentary component recycled in the Kef Lakhal mantle as shown in Fig. 11b. Whereas a combination of Pb and Nd isotopes does not allow distinguishing between Atlantic- or Pacific-like mantle sources, a combination of Nd and Hf isotopes (Fig. 9b) indicates that the source reservoir of the studied Kef Lakhal samples has a composition akin to the present day Pacific Ocean MORB. The weighted mean bulk rock εNd and εHf are undistinguishable within errors whatever the age correction and give values of 9.2 ± 0.5 and 9.4 ± 0.4 εNd unit (corrected at 40 and 150 Ma respectively), and 12.3 ± 1.3 and 12.0 ± 1.3 εHf unit (corrected at 40 and 150 Ma, respectively). These values further support that the Kef Lakhal mantle source was very close in composition to the depleted mantle, source of today's Pacific ($\varepsilon Nd = 9.4$ and $\varepsilon Hf = 13.2$) rather than Atlantic ($\varepsilon Nd = 8.3$ and $\varepsilon Hf = 14.8$) or Indian ($\varepsilon Nd = 7.7$ and $\varepsilon Hf = 13.7$) Ocean ridge basalts (all values after White and Klein, 2014). In this diagram it can also be noted that bulk rocks have a less radiogenic Hf with respect to a given Nd composition than the mantle array ($\varepsilon Hf = 1.33\ \varepsilon Nd + 3.19$ after Vervoort et al., 1999). This decoupling of Hf from Nd isotope ratios is attributed to recycling of oceanic crust and sediments (e.g., Geldmacher et al., 2011) which results in a time-integrated lowering of the $^{176}Hf/^{177}Hf$

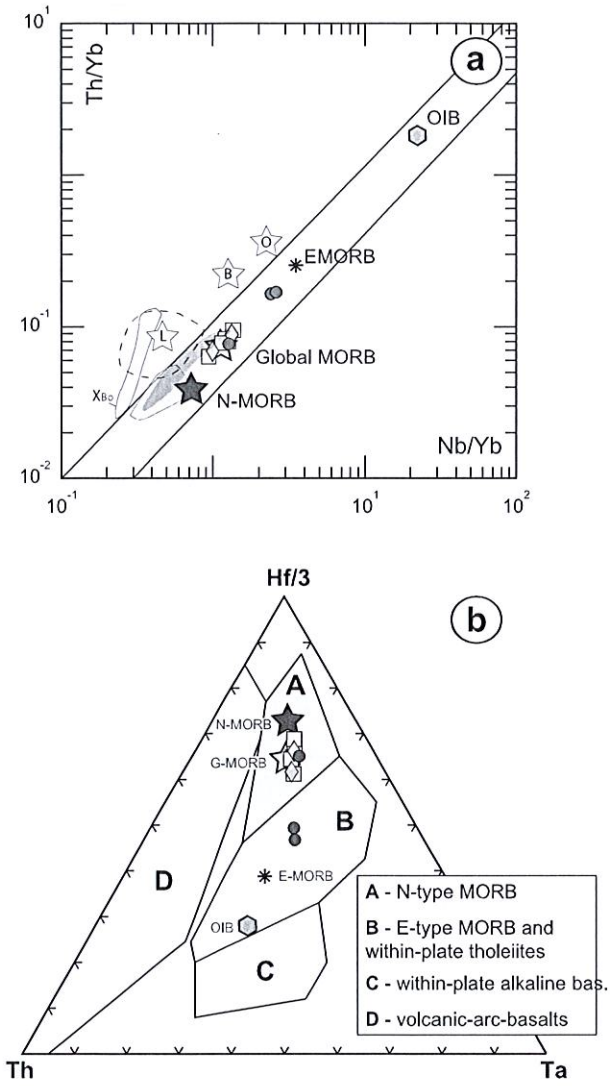

Fig. 10. (a) Th/Yb vs. Nb/Yb diagram (Pearce, 2008). N-MORB, *E*-MORB and OIB after Sun and McDonough (1989). Global MORB after Arevalo and McDonough (2010). Stars labelled B, L, and O are back-arc basin basalts: Global back-arc basin, Lau basin, and Okinawa Trough respectively (White and Klein, 2014). The grey field and yellow field are fore-arc basalts from the Mariana (Reagan et al., 2010) and Xigaze ophiolite (Dai et al., 2013), respectively. The empty dashed domain is back-arc basin basalts from the Mariana (Stern et al., 2013). XBo is the field of boninite from the Xigaze ophiolite (Dai et al., 2013). (b) Hf/3-Th-Ta ternary diagram (Wood, 1980). (For interpretation of the references to colour in this figure legend, the reader is referred to the web version of this article.)

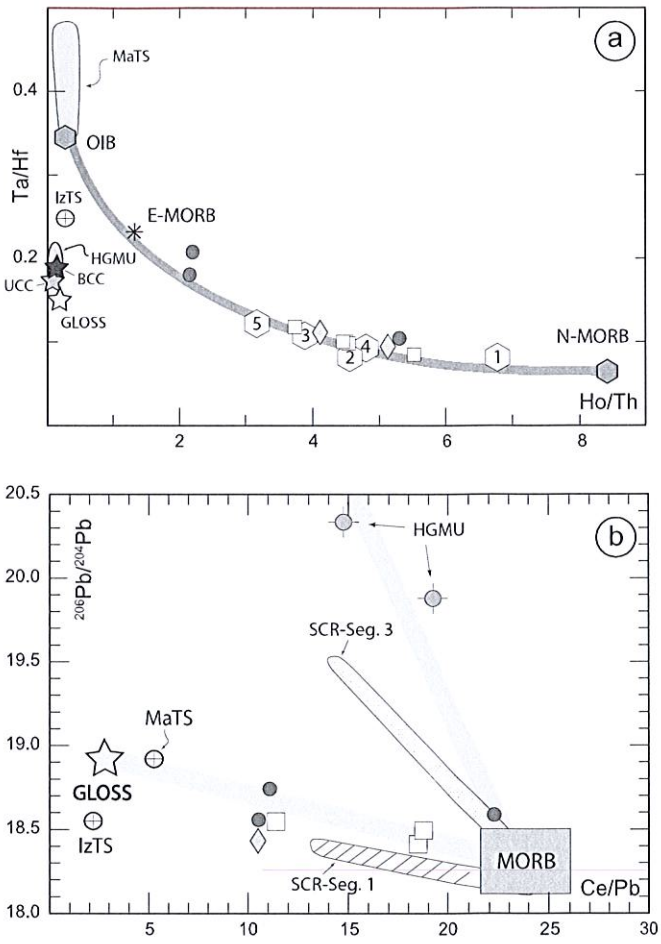

Fig. 11. (a) Ta/Hf vs. Ho/Th diagram (Niu and Batiza, 1997). E-MORB, N-MORB and OIB after Sun and McDonough (1989). Global MORB after Arevalo and McDonough (2010). Upper Continental crust (UCC) and Bulk Continental Crust (BCC) after Rudnick and Gao (2014). Empty hexagons are: 1 = Pacific MORB; 2 = Indian MORB; 3 = Atlantic MORB (White and Klein, 2014); 4 = Global MORB (Arevalo and McDonough, 2010); 5 = ALL MORB (Gale et al., 2013). HGMU (Edough Paleozoic terrigenous sediments) is from Fernandez et al., 2016. The Mariana volcaniclastic sediments at ODP sites 800 and 801 (MaTS), the Izu Trench sediments of mainly continental origin (IzTS) and GLOSS are from Plank and Langmuir (1998). For GLOSS, Izu trench and ODP sites 800 and 801, Ho has been calculated assuming no Ho anomaly ($Ho/Ho^* = 1$). The calculation gives Ho/Th values of 0.153, 0.240, 0.291 and 0.310 respectively. (b) $^{206}Pb/^{204}Pb$ vs. Ce/Pb diagram. GLOSS (Ce/Pb = 2.88 and $^{206}Pb/^{204}Pb = 18.913$) is from Plank and Langmuir (1998). SCR-Seg. 1 (recent contamination by sediment and altered oceanic crust) and SCR-Seg. 3 (ancient contamination or contamination by recently subducted old sediments) are South Chile Ridge Segment 1 and 3 respectively after Klein and Karsten (1995). HGMU (Edough Paleozoic terrigenous sediments) is from Fernandez et al., 2016. Limits of the MORB field are defined by Atlantic MORB (21.8 after White and Klein, 2014) and ALL-MORB (26.1 after Gale et al., 2013) for the Ce/Pb ratio and by Indian MORB (18.125 after White and Klein, 2014) and Pacific MORB (18.502 after White and Klein, 2014) for the $^{206}Pb/^{204}Pb$.

compared to $^{143}Nd/^{144}Nd$, the magnitude of which depends on the age of the recycled crust and associated sediments. Therefore, the Kef Lakhal samples can be explained by a mixture between a DMM-like mantle reservoir and small proportions of a young (<500 Myr-old) recycled oceanic crust along with overlying sediments.

6.4. Tectonic setting and implications for Mediterranean area evolution

Adding a sedimentary component to the asthenospheric mantle is most readily accomplished by mean of processes associated to subduction settings, where the altered oceanic crust and its sedimentary cover are recycled back into the mantle. These components can subsequently mix with MORB melts in four kinds of geodynamic environments.

Hot-spots sampling the deepest part of the mantle can bring back enriched components into the upper mantle. In today's oceanic basins, hot spots occur at many occurrences along the ridge segments and are responsible for eruption of melts with *E*-MORB and N-MORB signatures, although both kinds of MORB are common along plume-distal ridge segments too (Gale et al., 2013). The Kef Lakhal porphyroblastic amphibolites display E-MORB signatures (see Fig. 10b) which are consistent with this scenario. We note however that the timescale to recycle oceanic crust and sediments deep down into the mantle and back to the surface by mantle plumes has recently been revised to 200–650 Ma (Sobolev et al., 2011). Providing the addition of the sedimentary component in the Kef Lakhal samples occurred recently relative to the generation of the MORB melts, as suggested by Pb isotopes and trace elements (Figs. 11b and 14), this time scale is too long to envision such a contamination process in the mantle source of the Kef Lakhal rocks.

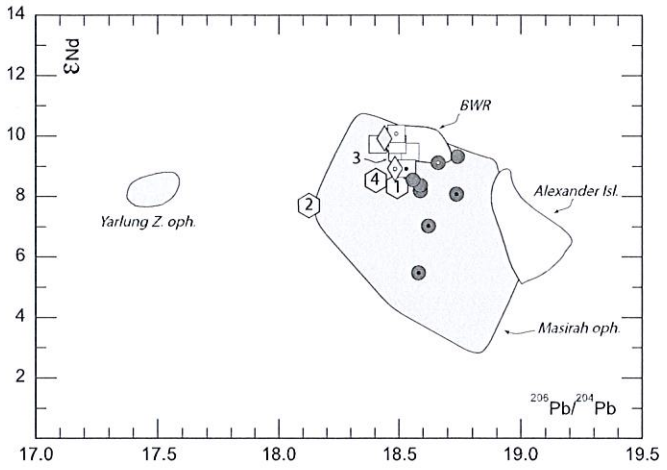

Fig. 12. εNd vs. $^{206}Pb/^{204}Pb$ diagram. Empty hexagons labelled 1, 2, 3 and 4 correspond to Atlantic, Indian, Pacific (White and Klein, 2014) and Global MORB (Arevalo and McDonough, 2010) respectively. The fields for Masirah, Alexander Island (Atlantic/Pacific Tethyan ophiolites) and Yarlung Zangpo (Indian-type Tethyan ophiolite) are from Mahoney et al. (1998). The field BWR refers to Kef Lakhal whole-rock analyses quoted in Bosch et al. (2014), age-corrected at 40 Ma.

Recycling of oceanic crust and sedimentary components also occurs in subduction-related environments such as arc systems, including fore- or back-arc basins (e.g. Ishizuka et al., 2006), or ridge subduction (e.g. Klein and Karsten, 1995). However, rocks formed in these settings are enriched in incompatible elements and depleted in HFSE (notably Nb and Ta relative to La and Th). They also display a tendency to plot outside the mantle array in the Th/Yb vs. Nb/Yb diagram (Fig. 10a). To our knowledge, rocks with a MORB-like signature formed in a subduction setting but without the associated typical HFSE depletion are known only in fore-arcs, such as the Mariana, where such lavas were formed during the earliest stages of the onset of subduction (Reagan et al., 2010), or in back-arcs that are located far behind the arc so that the subduction component is diluted and the mantle source is not significantly affected. Based on this similarity, we contend that the most likely origin for the Kef Lakhal Complex is that it was formed in a fore- or back-arc geodynamic setting. The use of the V vs. Ti/1000 diagram (Fig. 13) does not allow discriminating both settings, but suggests rather a slab-distal environment. We note however that, when compared to

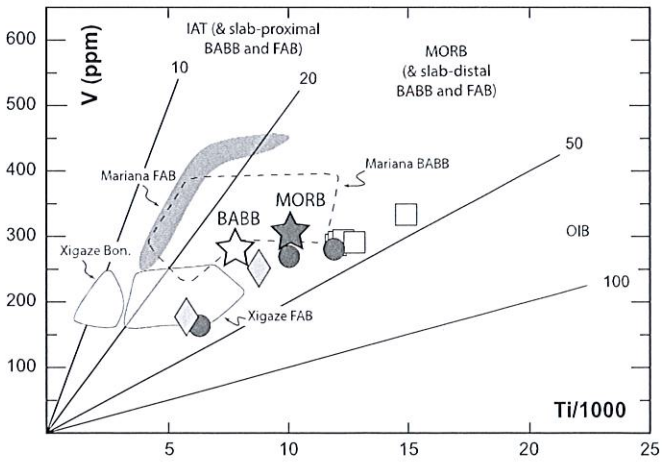

Fig. 13. V vs. Ti/1000 diagram (Shervais, 1982), modified after Pearce (2008). Mariana Fore-Arc Basalts (FAB) are from Reagan et al. (2010), Mariana Back-Arc Basin Basalts (BABB) are from Stern et al. (2013), Xigaze Boninite (Xigaze Bon.) and Fore-Arc Basalts (Xigaze FAB) are from Dai et al. (2013). BABB (empty star) is from White and Klein (2014).

occurrences of Mariana back-arc (Stern et al., 2013) or fore-arc (Reagan et al., 2010) rocks (Fig. 14), the Kef Lakhal samples display more affinities with fore-arc settings. In particular, as mentioned above we see no Nb—Ta depletion (relative to Th and La), which are frequent in back-arc basin products (e.g. Lau back-arc basin; White and Klein, 2014), no Th enrichments, and no positive Pb anomalies which result from slab fluxing during dehydration processes. We thus strongly favour a fore-arc environment for the Kef Lakhal complex and we review below the most likely geodynamic settings in which the complex may have developed.

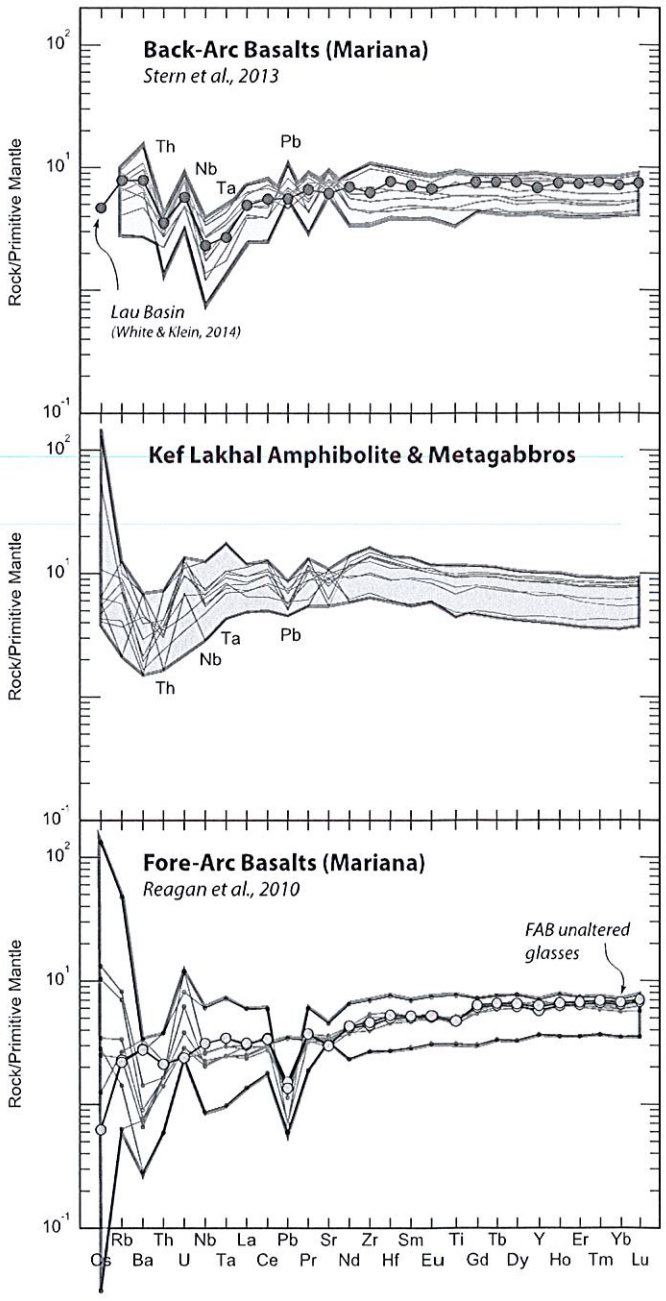

Fig. 14. Comparison of back-arc basalts (Stern et al., 2013) and fore-arc basalts (Reagan et al., 2010) from the Mariana and the Kef Lakhal samples. The spectrum of the Lau back-arc basin basalts is from White and Klein (2014). Note that, conversely to BABB, the Kef Lakhal samples do not show Nb—Ta negative anomalies, nor Pb positive spikes. LILE enrichments (Rb, Cs ± Ba) and U spikes are related to seawater alteration and not to addition of a subduction component.

The Western Mediterranean as a whole is a mosaic of (micro)plates and oceanic domains (for comprehensive reviews see Michard et al., 2006; Handy et al., 2010; Carminati et al., 2012; van Hinsbergen et al., 2014; Casciello et al., 2015; Lepretre et al., 2018) with a complex history of plate motions and interplay. From the literature above, there is a broad consensus that the Ligurian Ocean (and its northeastern prolongation, the Piedmontese Ocean) started opening during the Middle Jurassic times (~170–140 Ma; Tribuzio et al., 2016). Opening of the

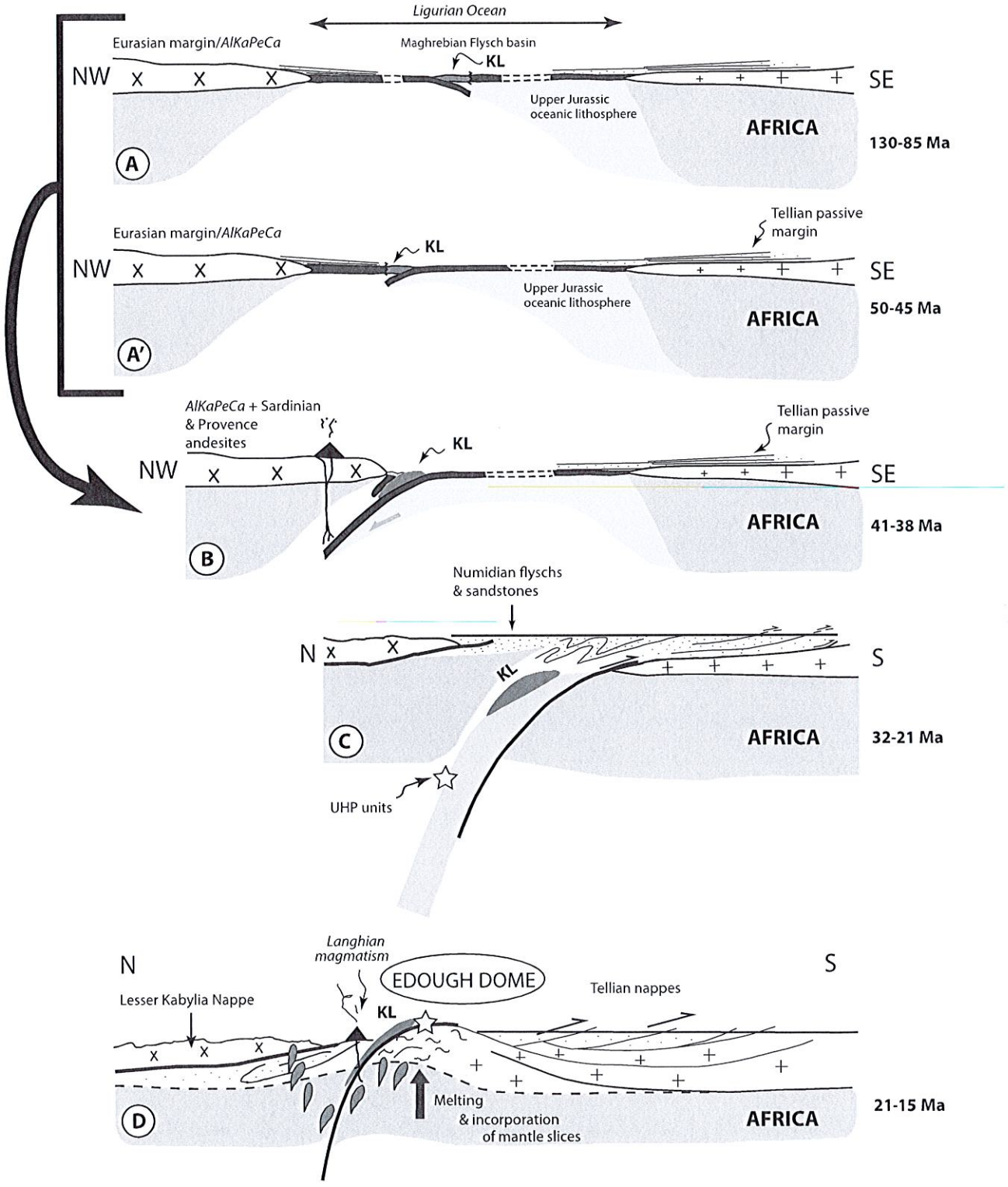

Fig. 15. Cartoon showing the scenario for the origin of the Kef Lakhal Complex in the context of the Western Mediterranean. Stages A and A' correspond to the two alternative possibilities for initiation of the Kef Lakhal fore-arc, either Cretaceous, or Middle Eocene. Stage A represents the East directed intra-oceanic subduction of the western part of the Ligurian Ocean occurring between 130 Ma and 85 Ma (Handy et al., 2010). Stage A' represents a flip of the subduction with the northwestward-directed subduction of the remnant of the Ligurian Ocean below the Iberia-Eurasia/*AlKaPeCa* margin taking place at around 45 Ma onward (Carminati et al., 2012). In the proposed scenario, this first stage (A or A') is followed by steps B, C and D. See text for explanation. KL stands for Kef Lakhal.

North Atlantic Ocean during the early Cretaceous (~130 Ma) was responsible for an eastward translation motion of Iberia (Handy et al., 2010). The counter-clockwise translation of Iberia lasted until the upper Cretaceous (~85 Ma; Vergés et al., 2019). Although this is a matter of debate, some auhors (e.g. Handy et al., 2010) proposed that the translation of Iberia triggered closure of the western part of the Ligurian Ocean by an east directed intra-oceanic subduction. Initiation of this intra-oceanic subduction is likely to have occurred along a transform fault consistently with the model of Stern and Bloomer (1992). This model also predicts formation of a fore-arc/back-arc system during strong extension of the overriding plate and the production of tholeiitic magmas during early magmatism in the fore-arc. This provides a consistent geodynamical setting to explain formation of the Kef Lakhal Complex. In this hypothesis, the most likely age of the Kef Lakhal Complex is bracketed between 130 and 85 Ma, thus Early to Late Cretaceous (Fig. 15A). Following the model of Stern and Bloomer (1992) and Whattam and Stern (2011), the negligible slab contribution (lack of HFSE depletion and of LILE enrichment), together with the MORB-like signature strongly suggest that the Kef Lakhal complex formed during subduction initiation, i.e. most likely during Early Cretaceous.

A major step in the Cenozoic evolution of the Western Mediterranean is related to a flip of subduction with the northwestward-directed subduction of the remnant of the Ligurian Ocean below the combined Iberia-Eurasia/*AlKaPeCa* margin. The onset of this event is still highly debated but could have started as early as Late Cretaceous at about 85 Ma (e.g. van Hinsbergen et al., 2014) or as late as Early Oligocene (Schettino and Turco, 2006). As already noted by Lustrino et al. (2009) a Late Cretaceous initiation of the subduction is difficult to reconcile with the age of the oldest arc volcanism in the Western Mediterranean which is dated at 38–41 Ma in Sardinia and Provence (Lustrino et al., 2009, 2017). This would imply a long delay of 45–50 Ma between subduction initiation and production of the first subduction-related magmatic products. A late initiation during the Early Oligocene is not valid either, for the same reason. The recent discovery of a diamond-bearing garnet megacryst in the Edough Massif attributed to deeply subducted slices of the Ligurian Ocean (Caby et al., 2014) with UHP metamorphism dated at ~32 Ma (Bruguier et al., 2017), is also consistent with this view. Collectively these data imply a subduction initiation not younger than ~40 Ma and most probably at around 45 Ma (Carminati et al., 2012). Interestingly, we note that between 67 and 35 Ma both the Adria and Africa plates display a north/northwestward motion (Handy et al., 2010) indicating that an important plate reorganisation took place during this time interval, that could have triggered the beginning of the northwestward subduction of the Ligurian Ocean below the European margin and the development of a Middle Eocene arc. In the Western Mediterranean, the most salient feature associated with the eastward roll-back of the Ligurian slab is the creation of a series of back arc basins in the overriding plate. In a preliminary study, Bosch et al. (2014) proposed that the Kef Lakhal Complex may represent remnants of the Liguro-Provençal back-arc basin (LPB). However, more recently, Fernandez et al. (2016) indicated that thrusting of the Kef Lakhal Complex occurred during the Aquitanian at 20.85 ± 0.34 Ma and was thus coeval with the onset of sea-floor spreading in the LPB (~ 21 Ma; Faccenna et al., 1997). Hence, linking the Kef Lakhal Complex with the southern termination of the Liguro-Provençal back-arc basin is not consistent with our present knowledge about the timing of sea-floor spreading in this basin or implies a very fast sequence of events that is very unlikely. In the Western Mediterranean, other occurrences of back-arc basins related to the southeastward rollback of the Ligurian slab (i.e. the Algerian Basin or the Tyrrhenian Sea) are even younger and therefore cannot fit with the time constraints provided by the Aquitanian thrusting of the Kef Lakhal units. It follows that a back-arc basin setting for the Kef Lakhal complex is very unlikely. This is in agreement with the trace element characteristics and only a fore-arc setting can be envisioned. Following the same reasoning of formation of fore-arc during subduction initiation, the age of the Kef Lakhal Complex may then be reduced to the oldest range of the proposed phase, i.e. more probably close to ~45 Ma, thus Middle Eocene (Fig. 15A').

Whatever the exact age of the Kef Lakhal Complex (i.e. Cretaceous or Middle Eocene; Fig. 15A and A'), we propose that amphibolite facies metamorphism was acquired during subduction of the fore-arc along with the oceanic lithosphere of the Ligurian Ocean. In the case of a Middle Eocene age, this requires that part of this fore-arc has been rapidly scrapped off and dragged down with the Ligurian slab (Fig. 15B). This slab reached a depth of ~100 km (the average depth of the top of the slab beneath arc volcanoes after Syracuse and Abers, 2006) at ~38–41 Ma (the age of the oldest arc magmatic products after Lustrino et al., 2009, 2017) (Fig. 15B) and then UHP conditions at ~32 Ma (Bruguier et al., 2017) (Fig. 15C). The Kef Lakhal fore-arc rocks were not buried that deep, and were brought back up and thrust onto the African paleomargin at ~21 Ma (Fernandez et al., 2016) before to finally cool to ~550 °C at 18.14 ± 0.27 Ma (this study) (Fig. 15D) during exhumation of the crust of the Edough Massif as a Metamorphic Core Complex (Bruguier et al., 2009; Caby et al., 2001).

7. Conclusion

The Kef Lakhal amphibolite unit exposed in the northern part of the Edough massif of NE Algeria is mainly composed of porphyroblastic and banded amphibolites along with metagabbros metamorphosed under amphibolite facies. The protolith of these rocks are tholeiitic basalts with MORB-like geochemical characteristics as evidenced by their trace element patterns and canonical inter-element ratios (i.e. Ti/Eu and Y/Ho) as well as Nd and Hf isotopic signatures typical of a DMM reservoir. This upper mantle source displays isotopic characteristics (high εNd and low εHf relative to Global MORB) akin to the present-day Pacific MORBs rather than to the Atlantic or Indian MORBs. $^{87}Sr/^{86}Sr$ isotopes (up to 0.70884), as well as enrichments in mobile elements (Cs, Rb and U), substantiate seawater alteration showing that the Kef Lakhal Complex represents a piece of altered oceanic crust. Pb isotopes and low Ce/Pb ratios further emphasise that the mantle reservoir was contaminated by a sedimentary component. Inter-element ratios rule out a terrigenous origin for the sediments but is consistent with a volcaniclastic component displaying high Ta/Hf and low Ho/Th, similar to sediments of today's Mariana fore-arc. In addition, relatively low $^{206}Pb/^{204}Pb$ ratios (18.4–18.8) combined with low Ce/Pb (down to ~10) are best explained by the sediments being added recently to the upper mantle source relative to the MORB genesis. These characteristics suggest an active setting nearby an intra-oceanic subduction zone. Comparison with fore-arc basalts from present day (Mariana) or fossil (Xigaze ophiolite) settings displays strong similarities suggesting that the Kef Lakhal Complex formed from near-trench magmatism occurring during the first stages of intra-oceanic subduction initiation. An overview of the geodynamic evolution of the Western Mediterranean indicates that fore-arc settings in the Ligurian Ocean realm could have formed either during the lower Cretaceous-Upper Cretaceous period or during the Middle Eocene. The Kef Lakhal Complex was subsequently subducted and metamorphosed under amphibolite facies conditions during the northwestward subduction of the Ligurian slab, before to be thrust onto the African margin during the Aquitanian (20.85 ± 0.34 Ma; Fernandez et al., 2016). $^{40}Ar/^{39}Ar$ ages on amphibole indicate that the Kef Lakhal fore-arc subsequently cooled down to ~550 °C at 18.14 ± 0.27 Ma.

Declaration of Competing Interest

The authors declare that they have no known competing financial interests or personal relationships that could have appeared to influence the work reported in this paper.

Acknowledgments

The authors are very grateful to M. Bonno and F. Lecoeur for their expertise in mass spectrometry, to B. Galland for the clean chemical

laboratory maintenance, to C. Nevado and D. Delmas for thin and thick section preparation and to B. Boyer for EPMA analyses. This work is part of the PhD work of L.F. which was supported by a MRT grant. We acknowledge funding by the INSU-SYSTER (2013 and 2014) Program to D.B., INSU-SYSTER (2016) Program to O.B. and by the CNRS-DPGRF France-Algeria Collaboration Program. The Badji Mokhtar University of Annaba is warmly thanked for its logistical support during the 2012 field trip in the Edough Massif. The authors are warmly grateful to Jin-Gen Dai, an anonymous reviewer and to the Editor Xian-Hua Li for their thorough reviews, which greatly improved the manuscript.

Appendix A. Supplementary data

Supplementary data to this article can be found online at https://doi.org/10.1016/j.lithos.2020.105649.

References

Ahmed-Said, Y., Leake, B.E., 1997. The petrogenesis of the Edough amphibolites, Annaba, NE Algeria: two unrelated basic magmas and the lherzolite-harzburgite residue of a possible magma source. Mineral. Petrol. 59, 207–237.

Arevalo, R., McDonough, W.F., 2010. Chemical variations and regional diversity observed in MORB. Chem. Geol. 271, 70–85.

Bach, W., Peucker-Ehrenbrink, B., Hart, S.R., Blusztajn, J.S., 2003. Geochemistry of hydrothermally altered oceanic crust: DSDP/ODP Hole 504B – implications for seawater – crust exchange budgets and Sr- and Pb-isotopic evolution of the mantle. Geochem. Geophys. Geosyst. 4. https://doi.org/10.1029/2002GC000419.

Ben Othman, D., White, W.M., Patchett, J., 1989. The geochemistry of marine sediments, island arc magma genesis, and crust-mantle recycling. Earth Planet. Sci. Lett. 94, 1–21.

Bosch, D., Hammor, D., Mechati, M., Fernandez, L., Bruguier, O., Caby, R., Verdoux, P., 2014. Geochemical study (major, trace elements and Pb–Sr–Nd isotopes) of mantle material obducted onto the North African margin (Edough Massif, North Eastern Algeria): Tethys fragments or lost remnants of the Liguro–Provençal basin? Tectonophysics 626, 53–68.

Bossière, G., Collomb, P., Mahdjoub, Y., 1976. Sur un gisement de péridotite découvert dans le massif de l'Edough (Annaba, Algérie). C. R. Acad. Sci. Paris 306, 1039–1045.

Bouillin, J.-P., 1986. Le "bassin maghrébin": une ancienne limite entre l'Europe et l'Afrique à l'Ouest des Alpes. Bull. Soc. Géol. Fr. 8–11, 547–558.

Bruguier, O., Hammor, D., Bosch, D., Caby, R., 2009. Miocene incorporation of peridotite into the Hercynian basement of the Maghrebides (Edough massif, NE Algeria): implications for the geodynamic evolution of the Western Mediterranean. Chem. Geol. 261, 172–184.

Bruguier, O., Bosch, D., Caby, R., Vitale-Brovarone, A., Fernandez, L., Hammor, D., Laouar, R., Ouabadi, A., Abdallah, N., Mechati, M., 2017. Age of UHP metamorphism in the Western Mediterranean: insight from rutile and minute zircon inclusions in a diamond-bearing garnet megacryst (Edough Massif, NE Algeria). Earth Planet. Sci. Lett. 474, 215–225.

Brun, J.P., Faccenna, C., 2008. Exhumation of high-pressure rocks driven by slab rollback. Earth Planet. Sci. Lett. 272, 1–7.

Caby, R., Hammor, D., Delor, C., 2001. Metamorphic evolution, partial melting and Miocene exhumation of lower crust in the Edough metamorphic core complex, West Mediterranean orogen, eastern Algeria. Tectonophysics 342, 239–273.

Caby, R., Bruguier, O., Fernandez, L., Hammor, D., Bosch, D., Mechati, M., Laouar, R., Ouabadi, A., Abdallah, N., Douchet, C., 2014. Metamorphic diamonds in a garnet megacryst from the Edough Massif (northeastern Algeria). Recognition and geodynamic consequences. Tectonophysics 637, 341–353.

Carminati, E., Wortel, M.J.R., Spakman, W., Sabadini, R., 1998. The role of slab detachment processes in the opening of the western–Central Mediterranean basins: some geological and geophysical evidence. Earth Planet. Sci. Lett. 160, 651–665.

Carminati, E., Lustrino, M., Doglioni, C., 2012. Geodynamic evolution of the central and western Mediterranean: Tectonics vs. igneous petrology constraints. Tectonophysics 579, 173–192.

Casciello, E., Fernandez, M., Verges, J., 2015. The Alboran in the western Mediterranean evolution: the birth of a concept. Bull. Soc. Geol. Fr. 186, 371–384.

Dahl, P.S., 1996. The effects of composition on retentivity of argon and oxygen in hornblende and related amphiboles: a field-tested empirical model. Geochim. Cosmochim. Acta 60, 3687–3700.

Dai, J., Wang, C., Polat, A., Santosh, M., Li, Y., Ge, Y., 2013. Rapid forearc spreading between 130 and 120 Ma: evidence from geochronology and geochemistry of the Xigaze ophiolite, southern Tibet. Lithos 172, 1–16.

Dercourt, J., Zonenshain, L.P., Ricou, L.E., Kazmin, V.G., Le Pichon, X., Knipper, A.L., Grandjacquet, C., Sbortshikov, I.M., Geyssant, J., Lepvrier, C., Pechersky, D.H., Boulin, B., Sibuet, J.-C., Savostin, L.A., Sorokhtin, O., Westphal, M., Bazhenov, M.L., Laurer, J.P., Biju-Duval, B., 1986. Geological evolution of the Tethys belt from the Atlantic to the Pamirs since the Lias. Tectonophysics 123, 241–315.

Doglioni, C., Gueguen, E., Sàbat, F., Fernandez, M., 1997. The western Mediterranean extensional basins and the Alpine orogen. Terra Nova 9, 109–112.

Faccenna, C., Mattei, M., Funiciello, R., Jolivet, L., 1997. Styles of back-arc extension in the Central Mediterranean. Terra Nova 9, 126–130.

Faccenna, C., Becker, T., Auer, L., Boschi, L., Brun, J.P., Capitanio, F.A., Funiciello, F., Horvath, F., Jolivet, L., Piromallo, C., Royden, L., Rossetti, F., Serpelloni, E., 2014. Mantle dynamics in the Mediterranean. Rev. Geophys. 52, 283–332.

Fernandez, L., Bosch, D., Bruguier, O., Caby, R., Monié, P., Arnaud, N., Galland, B., Toubal, A., Douchet, C., 2016. Permo-Carboniferous and early Miocene geological evolution of the internal zones of the Maghrebides – New insights on the Western Mediterranean evolution. J. Geodyn. 96, 146–173.

Gale, A., Dalton, C.A., Langmuir, C.H., Su, Y., Schilling, J.G., 2013. The mean composition of ocean ridge basalts. Geochem. Geophys. Geosyst. 14, 489–518.

Gattacceca, J., Deino, A., Rizzo, R., Jones, D.S., Henry, B., Beaudoin, B., Vadeboin, F., 2007. Miocene rotation of Sardinia: new paleomagnetic and geochronological constraints and geodynamic implications. Earth Planet. Sci. Lett. 258, 359–377.

Geldmacher, J., Hoernle, K., Hanan, B.B., Blichert-Toft, J., Hauff, F., Gill, J.B., Schmincke, H.U., 2011. Hafnium isotopic variations in East Atlantic intraplate volcanism. Contrib. Mineral. Petrol. 162, 21–36.

Handy, M.R., Schmid, S.M., Bousquet, R., Kissling, E., Bernoulli, D., 2010. Reconciling plate-tectonic reconstructions of Alpine Tethys with the geological-geophysical record of spreading and subduction in the Alps. Earth Sci. Rev. 102, 121–158.

Hart, S.R., 1988. Heterogeneous mantle domains: signatures, genesis and mixing chronologies. Earth Planet. Sci. Lett. 90, 273–296.

Hauff, F., Hoernle, K., Schmidt, A., 2003. Sr-Nd-Pb composition of Mesozoic Pacific oceanic crust (Site 1149 and 801, ODP Leg 185): Implications for alteration of ocean crust and the input into the Izu-Bonin-Mariana subduction system. Geochem. Geophys. Geosyst. 4. https://doi.org/10.1029/2002GC000421.

Holland, T., Blundy, J., 1994. Non-ideal interactions in calcic amphiboles and their bearing on amphibole-plagioclase thermometry. Contrib. Mineral. Petrol. 116, 433–447.

Humphris, S.E., Thompson, G., 1978. Hydrothermal alteration of oceanic basalts by seawater. Geochim. Cosmochim. Acta 42, 107–125.

Ishizuka, O., Kimura, J.I., Li, Y.B., Stern, R.J., Reagan, M.K., Taylor, R.N., Ohara, Y., Bloomer, S.H., Ishii, T., Hargrove, U.S., Haraguchi, S., 2006. Early stages in the evolution of Izu-Bonin arc volcanism: new age, chemical and isotopic constraints. Earth Planet. Sci. Lett. 250, 385–401.

Jolivet, L., Augier, R., Faccenna, C., Negro, F., Rimmele, G., Agard, P., Robin, C., Rossetti, F., Crespo-Blanc, A., 2008. Subduction, convergence and the mode of backarc extension in the Mediterranean region. Bull. Soc. Géol. Fr. 179, 525–550.

Jolivet, L., Faccenna, C., Huet, B., Labrousse, L., Le Pourhiet, L., Lacombe, O., Lecomte, E., Burov, E., Denèle, Y., Brun, J.P., Philippon, M., Paul, A., Salaun, G., Karabulut, H., Piromallo, C., Monié, P., Gueydan, F., Okay, A.I., Oberhansli, R., Pourteau, A., Augier, R., Gadenne, L., Driussi, O., 2013. Aegean tectonics: strain localisation, slab tearing and trench retreat. Tectonophysics 597, 1–33.

Kelley, K.A., Plank, T., Ludden, J., Staudigel, H., 2003. Composition of altered oceanic crust at ODP sites 801 and 1149. Geochem. Geophys. Geosyst. 4. https://doi.org/10.1029/202GC000435.

Kelly, A.E., Reuer, M.K., Goodkin, N.F., Boyle, E.A., 2009. Lead concentrations and isotopes in corals and water near Bermuda, 1780–2000. Earth Planet. Sci. Lett. 283, 93–100.

Klein, E., Karsten, J., 1995. Ocean-ridge basalts with convergent-margin geochemical affinities from the Chile Ridge. Nature 374, 52–57.

Kohn, M.J., Spear, F.S., 1990. Two new geobarometers for garnet amphibolites, with applications to southeastern Vermont. Am. Mineral. 75, 89–96.

Laouar, R., Boyce, A.J., Ahmed-Said, Y., Ouabadi, A., Fallick, A.E., Toubal, A., 2002. Stable isotope study of the igneous, metamorphic and mineralized rocks of the Edough complex, Annaba, Northeast Algeria. J. Afr. Earth Sci. 35, 271–283.

Le Bas, M.J., Le Maitre, R.W., Streckeisen, A., Zanettin, B., 1986. A chemical classification of volcanic rocks based on the total alkali-silica diagram. J. Petrol. 27, 745–750.

Leake, B.E., Woolley, A.R., Arps, C., Birch, W.D., Gilbert, M.C., Grice, J.D., Hawthorne, F.C., Kato, A., Kisch, H.J., Krivovichev, V.G., Linthout, K., Laird, J., Mandarino, J.A., Maresch, W.V., Nickel, E.H., Rock, N., Schumacher, J.C., Smith, D.C., Stephenson, N., Ungaretti, L., Whittaker, E., Youzhi, G., 1997. Nomenclature of amphiboles: report of the Subcommittee on Amphiboles of the International Mineralogical Association, Commission on new minerals and mineral names. Am. Mineral. 82, 1019–1037.

Lepretre, R., Frizon de Lamotte, D., Combier, V., Gimeno-Vives, O., Mohn, G., Eschard, R., 2018. The Tell-Rif orogenic system (Morocco, Algeria, Tunisia) and the structural heritage of the southern Tethys margin. Bull. Soc. Geol. Fr. 189, 10. https://doi.org/10.1051/bsgf/2018009.

Lustrino, M., Morra, V., Fedele, L., Franciosi, L., 2009. Beginning of the Apennine subduction system in central western Mediterranean: constraints from Cenozoic "orogenic" magmatic activity of Sardinia, Italy. Tectonics 28, TC5016. https://doi.org/10.1029/2008TC002419.

Lustrino, M., Duggen, S., Rosenberg, C.L., 2011. The Central-Western Mediterranean: anomalous igneous activity in an anomalous collisional tectonic setting. Earth Sci. Rev. 104, 1–40.

Lustrino, M., Fedele, L., Agostini, S., Di Vincenzo, G., Morra, V., 2017. Eocene-Miocene igneous activity in Provence (SE France): Ar-40/Ar-39 data, geochemical-petrological constraints and geodynamic implications. Lithos 288, 72–90.

Mahoney, J.J., Frei, R., Tejada, M.L.G., Mo, X.X., Leat, P.T., Nägler, T.F., 1998. Tracing the Indian Ocean mantle domain through time: isotopic results from old West Indian, East Tethyan, and South Pacific seafloor. J. Petrol. 39, 1285–1306.

Mauffret, A., Frizon de Lamotte, D., Lallemant, S., Gorini, C., Maillard, A., 2004. E-W opening of the Algerian Basin (western Mediterranean). Terra Nova 16, 257–264.

McCulloch, M.T., Gamble, J.A., 1991. Geochemical and geodynamical constraints on subduction zone magmatism. Earth Planet. Sci. Lett. 102, 358–374.

Mechati, M., Caby, R., Hammor, D., Bosch, D., Bruguier, O., Fernandez, L., 2017. Reworking of intra-oceanic rocks in a deep sea basin: example from the Bou-Maiza complex (Edough Massif, eastern Algeria). Int. Geol. Rev. https://doi.org/10.1080/00206814.2017.1343688.

Medaouri, M., Déverchère, J., Graindorge, D., Bracene, R., Badji, R., Ouabadi, A., Yelles-Chaouche, K., Bendiab, F., 2014. The transition from Alboran to Algerian basins (Western Mediterranean Sea): chronostratigraphy, deep crustal structure and tectonic evolution at the rear of a narrow slab rollback system. J. Geodyn. 77, 186–205.
Michard, A., Negro, F., Saddiqi, O., Bouybaouene, M.L., Chalouan, A., Montigny, R., Goffé, B., 2006. Pressure-temperature-time constraints on the Maghrebide mountain building: evidence from the Rif-Betic transect (Morocco, Spain), Algerian correlations, and geodynamic implications. C. R. Geosci. 338, 92–114.
Monié, P., Maluski, H., Montigny, R., 1992. A Burdigalian age for extensional ductile tectonics in the Edough Massif (Kabylies, Algeria). ^{39}Ar-^{40}Ar radiometric data. Bull. Soc. Geol. Fr. 163, 571–584.
Morimoto, N., 1988. Nomenclature of pyroxenes. Mineral. Petrol. 39, 55–76.
Niu, Y., Batiza, R., 1997. Trace element evidence from seamounts for recycled oceanic crust in the eastern Pacific mantle. Earth Planet. Sci. Lett. 148, 471–483.
Palmer, M.R., Edmond, J.M., 1989. Strontium isotope budget of the modern ocean. Earth Planet. Sci. Lett. 92, 11–26.
Pearce, J.A., 1996. A User's Guide to Basalt Discrimination Diagrams. 12. Geol. Assoc. Canada, pp. 79–113 Special Publication.
Pearce, J.A., 2008. Geochemical fingerprinting of oceanic basalts with applications to ophiolite classification and the search for Archean oceanic crust. Lithos 100, 14–48.
Pettke, T., Kodolanyi, J., Kamber, B.S., 2018. From ocean to mantle: new evidence for U-cycling with implications for the HIMU source and the secular Pb isotope evolution of the Earth's mantle. Lithos 316–317, 66–76.
Plank, T., Langmuir, C.H., 1998. The chemical composition of subducting sediment and its consequences for the crust and mantle. Chem. Geol. 145, 325–394.
Reagan, M.K., Ishizuka, O., Stern, R.J., Kelley, K.A., Ohara, Y., Blichert-Toft, J., Bloomer, S.H., Cash, J., Fryer, P., Hanan, B.B., Hickey-Vargas, R., Ishii, T., Kimura, J.I., Peate, D.W., Rowe, M.C., Woods, M., 2010. Fore-arc basalts and subduction initiation in the Izu-Bonin-Mariana system. Geochem. Geophys. Geosyst. 11, Q03X12. https://doi.org/10.1029/2009GC002871.
Rehkamper, M., Hofmann, A.W., 1997. Recycled Ocean crust and sediment in Indian Ocean MORB. Earth Planet. Sci. Lett. 147, 93–106.
Rudnick, R.L., Gao, S., 2014. Composition of the continental crust. In: Holland, H.D., Turekian, K.K. (Eds.), Treatise on Geochemistry, 2nd edition 4, pp. 1–51.
Schettino, A., Turco, E., 2006. Plate kinematics of the Western Mediterranean region during the Oligocene and Early Miocene. Geophys. J. Int. 166, 1398–1423.
Shervais, J.W., 1982. Ti-V plots and the petrogenesis of modern ophiolitic lavas. Earth Planet. Sci. Lett. 59, 101–118.
Sobolev, A.V., Hofmann, A.W., Jochum, K.P., Kuzmin, D.V., Stoll, B., 2011. A young source for the Hawaiian plume. Nature 476, 434–439.
Stampfli, G.M., Mosar, J., Marquer, D., Marchant, R., Baudin, T., Borel, G., 1998. Subduction and obduction processes in the Swiss Alps. Tectonophysics 296, 159–204.
Staudigel, H., Hart, S.R., Schminke, H.U., Smith, B.M., 1989. Cretaceous ocean crust at DSDP Sites 417 and 418: Carbon uptake from weathering versus loss by magmatic degassing. Geochem. Cosmochem. Acta 53, 3091–3094.
Stern, R.J., Bloomer, S.H., 1992. Subduction zone infancy: examples from the Eocene Izu-Bonin-Mariana and Jurassic California arcs. Geol. Soc. Am. Bull. 104, 1621–1636.
Stern, R.J., Tamura, Y., Masuda, H., Fryer, P., Martinez, F., Ishizuka, O., Bloomer, S.H., 2013. How the Mariana volcanic arc ends in the south. Island Arc 22, 133–148.
Sun, S.S., McDonough, W.F., 1989. Chemical and Isotopic Systematics of Oceanic Basalts: Implications for Mantle Composition and Processes. 42. Geol. Soc. London, pp. 313–345 Special Publications.
Syracuse, E.M., Abers, G.A., 2006. Global compilation of variations in slab depth beneath arc volcanoes and implications. Geochem. Geophys. Geosyst. 7. https://doi.org/10.1029/2005GC001045.
Tribuzio, R., Garzetti, F., Corfu, F., Tiepolo, M., Renna, M.R., 2016. U-Pb zircon geochronology of the Ligurian ophiolites (Northern Apennine, Italy): implications for continental break-up to slow seafloor spreading. Tectonophysics 666, 220–243.
van Hinsbergen, D.J., Vissers, R.L., Spakman, W., 2014. Origin and consequences of western Mediterranean subduction, rollback, and slab segmentation. Tectonics 33, 393–419.
Varas-Reus, M.I., Garrido, C.J., Marchesi, C., Bosch, D., Hidas, K., 2018. Genesis of ultra-high pressure garnet pyroxenites in orogenic peridotites and its bearing on the compositional heterogeneity of the Earth's mantle. Geochim. Cosmochim. Acta 232, 303–328.
Vergés, J., Kullberg, J.C., Casas-Sainz, A., de Vicente, G., Duarte, L., Fernàndez, M., Gómez, J.J., Gómez-Pugnaire, M.T., Sánchez, A., López-Gómez, J., Macchiavelli, J., Martín-Algarra, A., Martín-Chivelet, J., Muñoz, J., Quesada, C., Terrinha, P., Torné, M., Vegas, R., 2019. An introduction to the Alpine cycle in Iberia. In: Quesada, Oliveira (Eds.), The Geology of Iberia: A Geodynamic Approach, pp. 1–14.
Vervoort, J.D., Patchett, P.J., Blichert-Toft, J., Albarède, F., 1999. Relationships between Lu-Hf and Sm-Nd isotopic systems in the global sedimentary system. Earth Planet. Sci. Lett. 168, 79–99.
Vervoort, J.D., Plank, T., Prytulak, J., 2011. The Hf–Nd isotopic composition of marine sediments. Geochim. Cosmochim. Acta 75, 5903–5926.
Vignaroli, G., Faccenna, C., Jolivet, L., Piromallo, C., Rossetti, F., 2008. Subduction polarity reversal at the junction between the Western Alps and the Northern Apennines, Italy. Tectonophysics 450, 34–50.
Whattam, S.A., Stern, R.J., 2011. The 'subduction initiation rule': a key for linking ophiolites, intra-oceanic forearcs, and subduction initiation. Contrib. Mineral. Petrol. 162, 1031–1045.
White, W.M., Klein, 2014. Composition of the oceanic crust. In: Holland, H.D., Turekian, K.K. (Eds.), Treatise on Geochemistry, 2nd edition 4.13, pp. 457–496.
Wierzborwski, H., Anczkiewicz, R., Pawlak, J., Rogov, M.A., Kuznetsov, A.B., 2017. Revised Middle-Upper Jurassic strontium isotope stratigraphy. Chem. Geol. 466, 239–255.
Wood, D.A., 1980. The application of a Th-Hf-Ta diagram to problems of tectonomagmatic classification and to establishing the nature of crustal contamination of basaltic lavas of the British Tertiary volcanic province. Earth Planet. Sci. Lett. 50, 11–30.
Workman, R.K., Hart, S.R., 2005. Major and trace element composition of the depleted MORB mantle (DMM). Earth Planet. Sci. Lett. 231, 53–72.
Xu, J.F., Castillo, P.R., 2004. Geochemical and Nd–Pb isotopic characteristics of the Tethyan asthenosphere: implications for the origin of the Indian Ocean mantle domain. Tectonophysics 393, 9–27.